Research paper

Comparison of qualitative and quantitative dinoflagellate cyst approaches in reconstructing glacial-interglacial climate variability at West Iberian Margin IODP 'Shackleton' Site U1385

Mariska Datema[a,*], Francesca Sangiorgi[a], Anne de Vernal[b], Gert-Jan Reichart[c,d], Lucas J. Lourens[c], Appy Sluijs[a]

[a] Marine Palynology and Paleoceanography, Laboratory of Palaeobotany and Palynology, Department of Earth Sciences, Faculty of Geosciences, Utrecht University, Heidelberglaan 2, P.O. Box 80.115, 3508 TC Utrecht, The Netherlands
[b] Centre de recherche en géochimie et géodynamique (Geotop), Université du Québec à Montréal, P.O. Box 8888, Montréal, QC H3C 3P8, Canada
[c] Department of Earth Sciences, Faculty of Geosciences, Utrecht University, Heidelberglaan 2, P.O. Box 80.115, 3508 TC Utrecht, The Netherlands
[d] NIOZ Royal Netherlands Institute for Sea Research, Department of Ocean Systems, P.O. Box 59, 1790 AB Den Burg, Texel, The Netherlands

ARTICLE INFO

ABSTRACT

Dinoflagellate cysts (dinocysts) are commonly used to reconstruct past environmental conditions at the sea surface, such as primary production, temperature and salinity. Abundances of selected dinocyst taxa are used in qualitative indices, whereas the modern analogue technique (MAT) is used for quantitative reconstructions. Qualitative indices use process-based knowledge of present-day relations between the environmental variables and the distribution of dinocysts, whereas the MAT is based on the assumption that past assemblages have modern counterparts that correspond to similar sea-surface conditions. Here we explore the potential of both approaches to reconstruct sea surface temperature (SST), production (SSP), salinity (SSS) and seasonality during the last 22 thousand years along the West Iberian Margin (WIM), at Integrated Ocean Drilling Program (IODP) Site U1385. We compare results to published paleoclimatic reconstructions. Our SST and SSS reconstructions provide the first continuous dinocyst MAT-based SST and SSS records for this area and time interval.

Qualitative and quantitative dinocyst-based SST estimates from the WIM are similar and resemble previous SST estimates from dinocysts, alkenones and foraminifers from nearby sites. The surface temperature trends and millennial-scale variations largely match those from the Greenland ice core records. Quantitative MAT-based SST estimates show increased seasonality in the glacial stage resulting from strong winter cooling. Dinocyst MAT-based salinity decreases concomitantly with cooling during the Younger Dryas and Heinrich Stadial 1 (HS1), likely related to the melting of icebergs that reached the region during HS1. Our qualitative and quantitative SSP estimates show higher values in the glacial stage compared to the Holocene, which is consistent with published records and supports the usefulness of both approaches. Small differences between SST tracer records may be explained by the limited number of modern analogues from warm ocean regions in the dinocyst reference dataset for MAT, the small number of dinocysts used in the qualitative estimates, the possible effect of a parameter other than temperature that might amplify noise, and/or seasonal biases of the tracer species.

In any case, the advantage of the qualitative approach is to allow reconstructions in non-analogue situations. Regression of the qualitative index versus present-day SST also allows for a quantitative reconstruction, although over a limited range of SSTs (especially towards the lower end) and with quite some uncertainty, but produces reasonable values beyond the upper limit of the MAT. The MAT reconstructs more reliable SSTs, with a much smaller error of prediction, but only up to present-day WIM values, because it is based on the assumption that past assemblages have modern counterparts that correspond to similar sea-surface conditions, which is not always valid. The advantages of the MAT approach include its quantitative nature and insights into seasonality. Hence both approaches are complementary. At Site U1385, MAT can be used for reconstructions in the colder periods (YD, HS1 and glacial stage), with a small error of prediction and the quantified index can be used to estimate SST beyond the limit of the MAT (Holocene and B-A).

* Corresponding author.
E-mail addresses: M.C.Datema@uu.nl (M. Datema), F.Sangiorgi@uu.nl (F. Sangiorgi), devernal.anne@uqam.ca (A. de Vernal), G.J.Reichart@uu.nl (G.-J. Reichart), L.J.Lourens@uu.nl (L.J. Lourens), A.Sluijs@uu.nl (A. Sluijs).
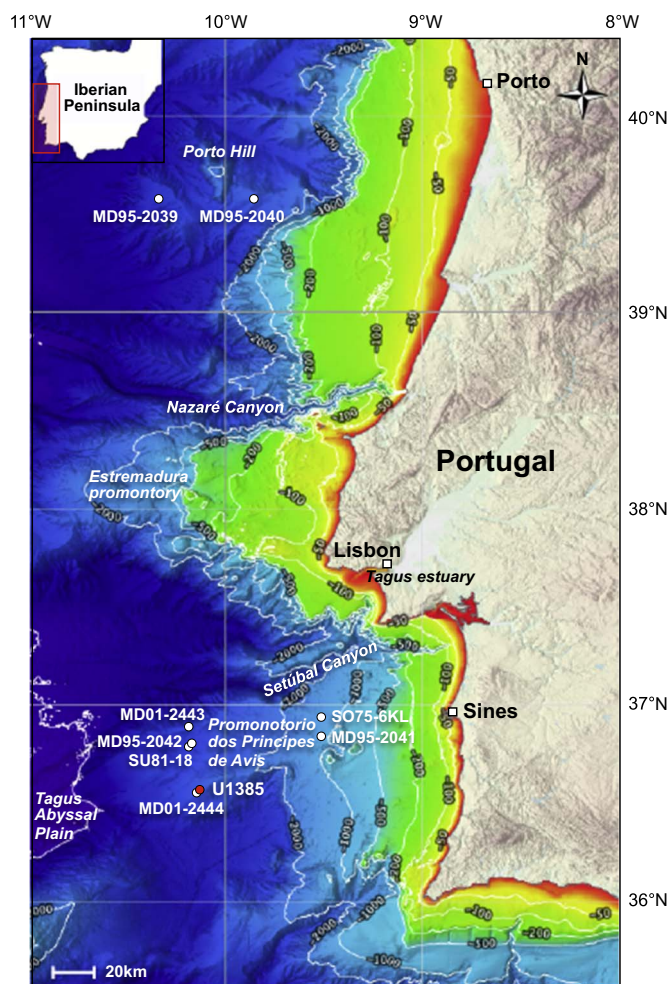
Fig. 1. Location of Shackleton Site U1385 and bathymetry of the (southern) West Iberian Margin. The Iberian Peninsula (inset adapted from Ribeiro et al., 2016), location of Shackleton Site U1385 (red circle) and other sites discussed in the text (white circles), depth (blue color for deeper zones), isobaths (50, 100, 200, 500, 1000 and 2000 m) and some of the main topographic features are shown. The bathymetric metadata and Digital Terrain Model data products have been derived from the EMODnet Bathymetry portal (http://www.emodnet-bathymetry.eu). (For interpretation of the references to color in this figure legend, the reader is referred to the web version of this article.)

1. Introduction

To understand the functioning of the climate system and the mechanisms underlying millennial-scale changes, sedimentary records that allow sufficiently high temporal resolution and tracers sensitive enough to capture these changes are needed. Ideally, the tracers should provide robust reconstructions of the important parameters of the climate system. Over the past decades, the West Iberian Margin (WIM), where several cruises retrieved sediment cores for paleoclimate reconstructions, proved to be an ideal location (Fig. 1). These cores provided high-resolution records of millennial-scale climate variability for the last glacial cycles (e.g. Martrat et al., 2007), which correlate very well to changes observed earlier in polar ice cores of both hemispheres and to existing European terrestrial climate records (e.g. Shackleton et al., 2000; Tzedakis et al., 2009).

Sediments from the WIM have been extensively studied for many time intervals using various (quantitative and qualitative) approaches and proxies, such as planktic foraminifera (e.g. Salgueiro et al., 2010; Voelker and de Abreu, 2011) and their isotopic composition (e.g. Shackleton et al., 2000, 2004; Eynaud et al., 2009), alkenones (e.g. Bard et al., 2000), pollen (e.g. Sanchez Goñi et al., 1999, 2000a, 2000b, 2002, 2006, 2008, 2009, 2013, 2016; Turon et al., 2003; Naughton

et al., 2007), and other (multi-proxy) studies (e.g. Pailler and Bard, 2002; de Vernal et al., 2006; Martrat et al., 2007; Penaud et al., 2011a, 2011b; Hodell et al., 2013a). The fossil remains of dinoflagellates (dinocysts) have also been successfully used to reconstruct past environmental conditions at the WIM (e.g. Zippi, 1992; Ribeiro and Amorim, 2008; Penaud et al., 2011a, 2011b; Ribeiro et al., 2016) and are commonly used to reconstruct past environmental conditions at the sea surface, including production (SSP), temperature (SST) and salinity (SSS).

Accurate reconstructions of past conditions ideally require process-based knowledge of the relations between the environmental variables and the distribution of dinocysts. On a global scale, a wealth of information on present-day dinocyst ecology is available (Zonneveld et al., 2013), which allows for qualitative reconstructions of environmental parameters based on taxa abundances. This approach is simple and can be used on long time scales, but does not provide quantitative results. For the Northern Hemisphere, a standardized database of present-day dinocyst assemblages and physico-chemical seawater parameters allows for quantification of paleoenvironmental conditions using the modern analogue technique (MAT) (Radi and de Vernal, 2008; de Vernal et al., 2001, 2005, 2013a, 2013b). In addition, this database can be used to verify and quantify the relation between present-day dinocyst abundances and SST. However, these quantitative estimates are based on the assumption that the past assemblages have modern counterparts that correspond to similar sea-surface conditions, which may not always be valid. All approaches thus have advantages and limitations.

Our principal aim is to compare qualitative and quantitative approaches to explore their potential to reconstruct the glacial-interglacial climate and environmental variability. We use sediments deposited over the last 22 thousand years (kyr) along the WIM, recovered during Integrated Ocean Drilling Program (IODP) Expedition 339 at Site U1385 (Hodell et al., 2013a). To this end we have generated sea surface temperature (warm/cold SST_{dino} index) and production estimates based on a qualitative approach (dinocyst abundances) and SST_{MAT}, SSS_{MAT}, SSP_{MAT} and seasonality based on MAT applied to the Modern n = 1492 database of de Vernal et al. (2013a). In addition, we use the n = 1492 database to quantify the relation between present-day SST_{dino} and SST to reconstruct quantitative SST from the index as a third approach. We compare these qualitative and quantitative dinocyst-based estimates to each other and to existing reconstructions, based on dinocysts, foraminifera, alkenones and oxygen isotopes, from nearby sites.

Studies that report winter SSTs in addition to summer and/or annual SSTs along the WIM are rare. Therefore, we generate a qualitative SST_{dino} record that we compare to quantitative summer SST (SST_{MATsu}) and winter SST (SST_{MATwi}) as well as to independent SST records that may yield a seasonal bias. Importantly, we also present new reconstructions of sea surface salinity (SSS_{MAT}) for the last 22 kyr at the WIM. Approaches to reconstruct salinity are not straightforward and paleosalinity records along the WIM are rare. Although dinocyst assemblages permit salinity estimates (e.g. de Vernal et al., 2001, 2005), only few dinocyst publications from the WIM provide SSS reconstructions (e.g. Penaud et al., 2011a). In addition, we document variability in production over the last glacial-interglacial transition, using accumulation rates of cysts resistant to oxidative degradation and MAT-based SSP reconstructions (SSP_{MAT}). We present a critical evaluation of the advantages and limitations of the different tracers used for paleoclimatic and paleoceanographic reconstructions along the WIM.

2. Oceanographic setting of the West Iberian Margin

2.1. Present-day oceanography

In the North Atlantic Ocean, the Polar Front separates cold low-salinity Polar Water, characterized by seasonal sea ice and iceberg drift, from warm, high-salinity Atlantic Water (e.g. Eynaud et al., 2009). The
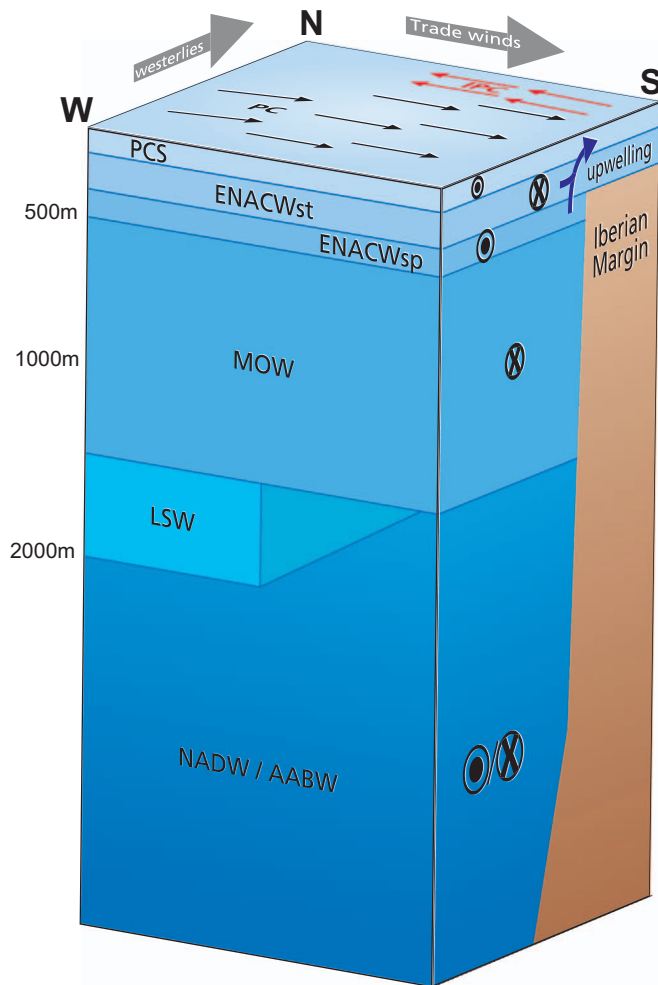
Fig. 2. Schematic representation of atmospheric and oceanographic components of the West Iberian Margin upwelling system. Adapted from Pailler and Bard (2002), Bischof et al. (2003) and Sprangers et al. (2004). Gray arrows represent westerly and northerly winds. Black arrows indicate the general flow direction of the Portugal Current (PC), while red arrows indicate flow direction of the Iberian Poleward Current (IPC), mostly active on the continental shelf in winter (Section 2.1). PCS = Portugal Current System, ENACW = Eastern North Atlantic Central Water, with a subtropical and subpolar component, MOW = Mediterranean Outflow Water, LSW = Labrador Sea Water, NADW = North Atlantic Deep Water, AABW = Antarctic Bottom Water. Vertical stratification is seasonally variable: the mixed layer is deeper in winter and reaches up to 200 m depth in March (Teles-Machado et al., 2015a). (For interpretation of the references to color in this figure legend, the reader is referred to the web version of this article.)

North Atlantic Eastern Boundary Current determines the main regional currents along the WIM (Peliz et al., 2005; Relvas et al., 2007). The large-scale Portugal Current System (PCS) represents surface waters (Fig. 2), with the offshore slow Portugal Current (PC) flowing towards the south (Arístegui et al., 2005; Teles-Machado et al., 2015b) and direction of flow over the narrow continental shelf changing seasonally (Peliz et al., 2005; Teles-Machado et al., 2015a). In summer (July--September), the Azores High is strong and shifts towards the northwest, which causes an increase in the intensity and steadiness of the northerly Portuguese Trade Winds (Relvas et al., 2007). Consequently, the PC flows southward over the shelf, which induces upwelling as a result of offshore Ekman transport (Arístegui et al., 2009). Filaments of upwelled cool and nutrient-rich water sometimes extend offshore over hundreds of kilometers at promontories and canyons and fuel primary production (Relvas et al., 2007).

In winter, the Azores High is weak and shifts towards the south, close to the Iberian Peninsula, causing a dominance of westerly/southerly winds (Relvas et al., 2007; Teles-Machado et al., 2015a). In combination with currents induced by river plumes, which are more frequent in winter, this results in intensification of the northward Iberian Poleward Current (IPC) from September to January, which transports warm and salty waters (Teles-Machado et al., 2015a, 2015b) and ceases upwelling (Arístegui et al., 2009). In this situation, the Western Iberia Winter Front, located between 10 and 11°W, separates the subtropical IPC waters from the cooler PC (Peliz et al., 2005). The IPC is present throughout most of the year, but is situated closer to the shelf-break and is overlain by the southward upwelling current in summer (Teles-Machado et al., 2015a).

Below the seasonally variable PCS (~ 100 m) a layer of Eastern North Atlantic Central Water (ENACW) supplies upwelled waters (Fig. 2). The ENACW consists of two components: a northward flowing relatively warm, fresh and nutrient-poor subtropical component (ENACW$_{st}$, ~ 200–300 m) and a southward flowing colder, more saline, nutrient-richer subpolar component (ENACW$_{sp}$, ~ 300–400 m), which reaches the sea surface only during strong upwelling events (Arístegui et al., 2005). Between ~ 500 and 1500 m, relatively warm and saline northward flowing Mediterranean Outflow Water (MOW) dominates the water column (Stow et al., 2011). Labrador Sea Water (LSW) flows beneath the MOW north of 40.5°N (Álvarez et al., 2004). Below 2000 m, the thermohaline equilibrium between the North Atlantic Deep Water (NADW) and Antarctic Bottom Water (AABW) controls the prevailing deep-water masses (Skinner and Shackleton, 2004; Stow et al., 2011). At present, the NADW dominates deep waters at U1385, although southern-sourced waters reached the site during glacial periods (Hodell et al., 2013a).

Modern sea surface summer temperatures (SST$_{su}$) average 20.4 ± 0.2 °C, while winter temperatures (SST$_{wi}$) are 15.3 ± 0.2 °C, implying a seasonal difference of ~ 5.1 °C; SSS is uniform throughout the year with values of $\sim 36.2 \pm 0.1$ (World Ocean Database: Boyer et al., 2013); mean annual production (SSP) is 347.3 gC m^{-2} yr^{-1} (compiled from MODIS satellite observation, http://modis.gsfc.nasa.gov/). Note that these are local seasonal averages near Site U1385 and that sea surface parameters can vary locally and on shorter time scales due to variable spatial extent of upwelling filaments and meandering extensions of modern sea surface fronts (Peliz et al., 2005).

2.2. Paleoceanographic and paleoclimatological changes across the last deglaciation

Regional sea level rise during the last deglaciation was ~ 55 m (Leorri et al., 2013). This implies a glacial coastline only ~ 3 km closer to Site U1385 than at present (Fig. 1), hence the water depth and distance to the coast of Site U1385 during the last glacial stage did not substantially differ from present-day (~ 115 km off the coast, water depth of 2578 m, Section 3.1). Southward extension of ice sheets during the glacial resulted in a more zonal and southward position of the Azores high and Polar Front, which probably caused an increase in the intensity and steadiness of the northerly Portuguese Trade Winds (Pailler and Bard, 2002). This possibly increased the intensity, persistence and/or spatial extent of the upwelling filaments along the WIM (e.g. Pailler and Bard, 2002; Voelker et al., 2009; Salgueiro et al., 2010, 2014), resulting in the observed high SSP in the last glacial stage (e.g. Penaud et al., 2011b; Salgueiro et al., 2010, 2014). The Last Glacial Maximum (LGM) was also characterized by a stronger seasonal SST contrast than at present, with more negative SST anomalies in winter than in summer (de Vernal et al., 2005, 2006). LGM SSS in the North Atlantic and near Site U1385 were lower than at present by a few units in response to freshwater discharge from the surrounding Fennoscandian and Laurentide ice sheets (de Vernal et al., 2005, 2006).

Although the Polar Front, which physically constrains sea ice and iceberg drifting, shifted southward, it did generally not reach the WIM during the LGM (e.g. Eynaud et al., 2009). Melting icebergs and subarctic waters only reached the WIM during the Greenland Stadials (GS) of the Last Glacial, including Heinrich Stadials (HS) and the Younger

Dryas (YD) (Cayre et al., 1999; Bard et al., 2000; de Vernal et al., 2013a, 2013b; Eynaud et al., 2009; Salgueiro et al., 2014). During Heinrich Events (HEs) the Polar Front oscillated around ~40°N along the WIM and Arctic and subarctic waters and icebergs penetrated the area as far south as 36°N (e.g. Eynaud et al., 2009; Voelker and de Abreu, 2011). This resulted in colder conditions and lower SSS in Heinrich Stadial 1 (HS1) with respect to the LGM (e.g. Cayre et al., 1999; Bard et al., 2000; Martrat et al., 2007; Eynaud et al., 2009; Voelker and Abreu, 2011; Darfeuil et al., 2016). In the Younger Dryas (YD) the protrusion of northern waters to the WIM was probably limited to subarctic waters (Eynaud et al., 2009), hence the YD was a cold and low SSS event compared to the B-A and Holocene, but not as much as during HS1. In the Holocene SSTs and SSS were generally high and SSP low (e.g. Cayre et al., 1999; Pailler and Bard, 2002; Salgueiro et al., 2014; Darfeuil et al., 2016).

3. Material and methods

3.1. Site U1385

IODP "Shackleton" Site U1385 (37°34.285′ N, 10°7.562′ W) is situated along the WIM (Fig. 1), within the band characterized by seasonal coastal upwelling. The steep upper slope of the shelf is intersected by promontories and indented by canyons (e.g. Setúbal Canyon), while seamounts occur on the lower slope and continental rise (van Weering et al., 2002). The Tagus River flows into the North Atlantic near Lisbon. The narrow continental shelf of the WIM leads to rapid delivery of terrestrial material to the deep basin (Hodell et al., 2013a). Site U1385 is located ~115 km off the nearest coast on the Promontório dos Príncipes de Avis on the continental slope of the southwestern Iberian Margin (Hodell et al., 2013a). The drill site is located at a water depth of 2578 m, hence above the influence of turbidite sedimentation and beyond the reach of the MOW (Hodell et al., 2013a).

A continuous sediment record spanning the past ~1.45 Ma was recovered at Site U1385, without hiatuses in the interval encompassing the last 22 kyr (Hodell et al., 2015). The sediment consists of nannofossil muds and clays, with varying proportions of biogenic carbonate and terrigenous components (Expedition 339 Scientists, 2013). A total of 56 samples were taken every 10 cm from the uppermost 4.55 meter composite depth (mcd) of the A/B splice (Appendix A: Table A1), which represents the last 22 kyr based on the reference time scale of Site U1385 from Hodell et al. (2015).

3.2. Age model for Site U1385

Barker et al. (2011) produced a synthetic Greenland $\delta^{18}O$ temperature record (GL_T_syn) based on the δD temperature record of the Antarctic EPICA Dome C (EDC) ice core and placed it on the absolutely dated Asian speleothem record of Cheng et al. (2009). Hodell et al. (2013b) tied the planktic foraminifer $\delta^{18}O$ record from Site MD01-2444 to this synthetic Greenland temperature record. Site MD01-2444 (37°33.88′ N, 10°8.34′ W, at 2656 m water depth) is practically at the same location as Site U1385 (Fig. 1), which Hodell et al. (2015) therefore easily correlated to MD01-2444 based on Ca/Ti records. This implies a high-accuracy dating of Site U1385 on the whole, although the here studied part of the record (last 22 kyr) contains only four tie points between Sites MD01-2444 and U1385 (Appendix B: Fig. B1). The resulting average sedimentation rate over the last 22 kyr is ~20 cm/kyr. We calculated ages for the 56 sampled intervals using linear interpolation between the four tie points (Appendix B: Fig. B2).

Note that timing of changes in tracers might be offset between the Greenland ice core, MD01-2444 and U1385, because these three sites are correlated only through a few tie points in the studied interval (Appendix B: Fig. B1). Therefore, we defined the Holocene, stadials and interstadials based on events in the tracer records, not on absolute timing of events. We use the definition and numbering of Greenland

Stadials (GS) and Interstadials (GI) following the updated INTIMATE event stratigraphy of Rasmussen et al. (2014) that is based on the synchronization of the NGRIP, GRIP, and GISP2 ice-core records. We name the WIM equivalents of the GS and GI Iberian Margin Stadials (IMS) and Interstadials (IMI), following Martrat et al. (2007), but assign the numbering of their Greenland equivalents (Rasmussen et al., 2014), assuming that the Greenland and WIM stadials and interstadials are contemporaneous (Wolff et al., 2010), since U1385 ages are based on the Greenland age model. Hence, IMS-1 and IMS-2.1a are the WIM equivalents of GS-1 and GS-2.1a. The Younger Dryas (YD) and Bølling-Allerød (B-A) are the terrestrial equivalents of IMS-1 and IMI-1, respectively. This terminology is widely used, although these events were originally defined in and should therefore be restricted to terrestrial records, strictly speaking. We use the YD and B-A to also refer to IMS-1 and IMI-1, for convenience, thereby following the recommendations of Rasmussen et al. (2014). During some GS/IMS, Heinrich Events (HEs) occurred. We use the term Heinrich Stadial (HS) to refer to an entire stadial containing a particular Heinrich Event (with the numbering following that of the HE) following Sanchez Goñi and Harrison (2010) and Rasmussen et al. (2014). We use the definition of the Holocene as the end of GS-1/IMS-1/the YD following Walker et al. (2009).

Comparison of the Greenland, Site MD01-2444 and Site U1385 records suggests that there is a discrepancy around GS/IMS-1 (Appendix B: Fig. B1). GS-1 lasts ~1500 years in the synthetic Greenland $\delta^{18}O$ record of Barker et al., 2011 (Appendix B: Fig. B1A). The extent of IMS-1 in the Ca/Ti record of Site MD01-2444 is 0.12 m, which would represent 750 years based on the age model of Hodell et al. (2013b) (Appendix B: Fig. B1B). For Site U1385, linear interpolation between the first two tie points of the age model of Hodell et al. (2015) at 0.91 and 11.71 ka results in a sedimentation rate of ~17 cm/kyr (Appendix A: Table A1; Appendix B: Fig. B2). Consequently, IMS-1 in the Ca/Ti record of Site U1385 (0.32 m) would represent 1850 years. Sites MD01-2444 and U1385 are very close to each other (Fig. 1), hence the timing of variations in the Ca/Ti record should be similar. Taking into account the linear sedimentation rate at Site U1385, the duration of IMS-1 would be similar to that of GS-1, which may suggest that the compressed expression of IMS-1 results from a hiatus and/or condensed section in the record of MD01-2444. Therefore, the position of the tie points correlating the Greenland ice core and sites MD01-2444 and U1385 and this apparent discrepancy result in a relatively young YD age at Site U1385.

3.3. Palynological processing

Approximately 13 g of sediment per sample were processed following the standard quantitative palynological procedure at the Laboratory of Palaeobotany and Palynology of Utrecht University, which includes 10% HCl and 38% cold HF treatment and sieving over a 10 μm mesh sieve (see van Helmond et al., 2015 for details), but no acetolysis or oxidation (see Zonneveld et al., 2008). These preparation techniques are the same as those adopted for the development of the standardized Northern Hemisphere database (e.g. Rochon et al., 1999; de Vernal et al., 2001, 2005, 2013a). Dinocysts were identified to the genus or species level, following the taxonomy of Rochon et al. (1999), Williams et al. (2017) and Zonneveld and Pospelova (2015). Microscopic slides were counted at 400× magnification to an average of ~470 dinocysts per sample (minimum of 371 and maximum of 1350), with the objective to achieve the highest counts possible for the taxa used for SST reconstructions (Table 1). All samples and slides are stored in the collection of the Laboratory of Palaeobotany and Palynology, Utrecht University, the Netherlands. Percentages of dinocysts are calculated using the total dinocyst sum, which includes all dinocysts excluding rare, reworked and unidentified specimens. Dinocyst accumulation rates (dinocysts $cm^{-2} yr^{-1}$) were calculated multiplying the amount of dinocysts per gram sediment dry weight by the mass accumulation rates (g $cm^{-2} yr^{-1}$).

Table 1

Grouping of dinocyst taxa according to their ecological preferences. See Section 3.4 for details.

Dinocysts	
Warm	Cold
Impagidinium paradoxum	*Bitectatodinium tepikiense*
Impagidinium patulum	*Impagidinium sphaericum*
Impagidinium strialatum	Cysts of *Pentapharsodinium dalei*
Operculodinium israelianum	*Spiniferites elongatus*
Tuberculodinium vancampoe	

3.4. Qualitative environmental tracers based on dinocysts

We assess relative variations in surface water parameters based on selected dinocyst taxa (Table 1) following previous work done in the area (Boessenkool et al., 2001; Ribeiro and Amorim, 2008; Eynaud et al., 2016 and references therein) and the global geographic distribution of modern dinocysts in surface sediments (Zonneveld et al., 2013 and references therein). The SST_{dino} index is defined as: $SST_{dino} = n_w/(n_w + n_c)$, where n_w = number of 'warm' taxa cysts and n_c = number of 'cold' taxa cysts counted (see Table 1 for composition of these groups). 'Warm' and 'cold' are relative to present-day SST at the WIM (Section 2.1). All dinocyst taxa that typically relate to high productivity and/or upwelling (including mostly heterotrophs) are excluded from the SST index to avoid an overprint of productivity on SST_{dino}. However, in the modern ocean, our 'warm' and 'cold' taxa also have specific ranges regarding SSS (Zonneveld et al., 2013). Although the influence of SST on SST_{dino} is expected to be dominant, there may be a minor SSS effect on SST_{dino}. To test how the index relates to SST, SSS and SSP, we calculate our SST_{dino} on the modern Northern Hemisphere assemblages from the surface sediment dataset of de Vernal et al. (2013a) and regress it against the available sea surface parameters of the same samples (summer/winter SST and SSS and SSP, Appendix C).

We also use the relation between SST_{dino} and SST to quantify summer and winter SST from the qualitative SST_{dino} index (SST_{dinosu}

and SST_{dinowi} in °C). To this end, we select all samples from the dataset of de Vernal et al. (2013a) for 15 °C (SST_{su}, n = 263) and 7 °C (SST_{wi}, n = 285) and higher. Index values are 0 below these SSTs (Appendix C: Fig. C1B–C). To emphasize the general trends we group SST into bins of equal size (n = 26 and n = 29 for SST_{su} and SST_{wi}, respectively) and calculate the average (arithmetic mean) of SST and the dinocyst index within each bin. We calculate linear regressions between the qualitative SST_{dino} and present-day summer and winter SST on the binned data (Fig. 3). Subsequently, we calculate summer and winter SST for the last 22ky from the qualitative SST_{dino} index at Site U1385 using these regressions (Fig. 3; $SST_{dinosu} = (SST_{dino} + 1.4443) / 0.098$, $SST_{dinowi} = (SST_{dino} + 0.9287) / 0.1155$). Consequently, the possible ranges in SST that can be reconstructed using these quantifications are 14.74–24.94 °C for SST_{dinosu} and 8.04–16.70 °C for SST_{dinowi}.

Palynomorph accumulation rates are influenced by both production and preservation. Dinocysts show differences in sensitivity to oxidative degradation, which is assumed to be related to differences in the chemical composition of cyst walls (Zonneveld et al., 2007; Bogus et al., 2012). Zonneveld et al. (2007) observed a significant exponential decrease of the accumulation rate of cysts that are sensitive to oxidative degradation (S-cysts) with bottom water oxygen concentration, but an insignificant relationship with upper water chlorophyll-*a* concentrations. In contrast, the accumulation rate of cysts resistant to oxidative degradation (R-cysts) showed a significant linear increase with upper water chlorophyll-*a* concentrations, but no significant relationship with bottom water oxygen concentration (Zonneveld et al., 2007). Hence, we use the accumulation rate of R-cysts as tracer for past SSP.

We quantify degradation using an index based on dinocysts with different degradation potentials (Appendix A: Table A1; Appendix D: Table D1). This so-called kt-index is a ratio between the expected initial number of S-cysts (calculated from the measured amount of R-cysts in the samples, assuming a fixed relation between S- and R-cyst production (Zonneveld and Brummer, 2000; Zonneveld et al., 2007, 2008)) and the actual number of S-cysts in the samples: $kt = \ln(X_i / X_f)$, where kt is a dimensionless measure of dinocyst degradation, $X_i = 68 * X\text{-}r$ = initial accumulation rate of S-cysts (cysts $cm^{-2} yr^{-1}$),
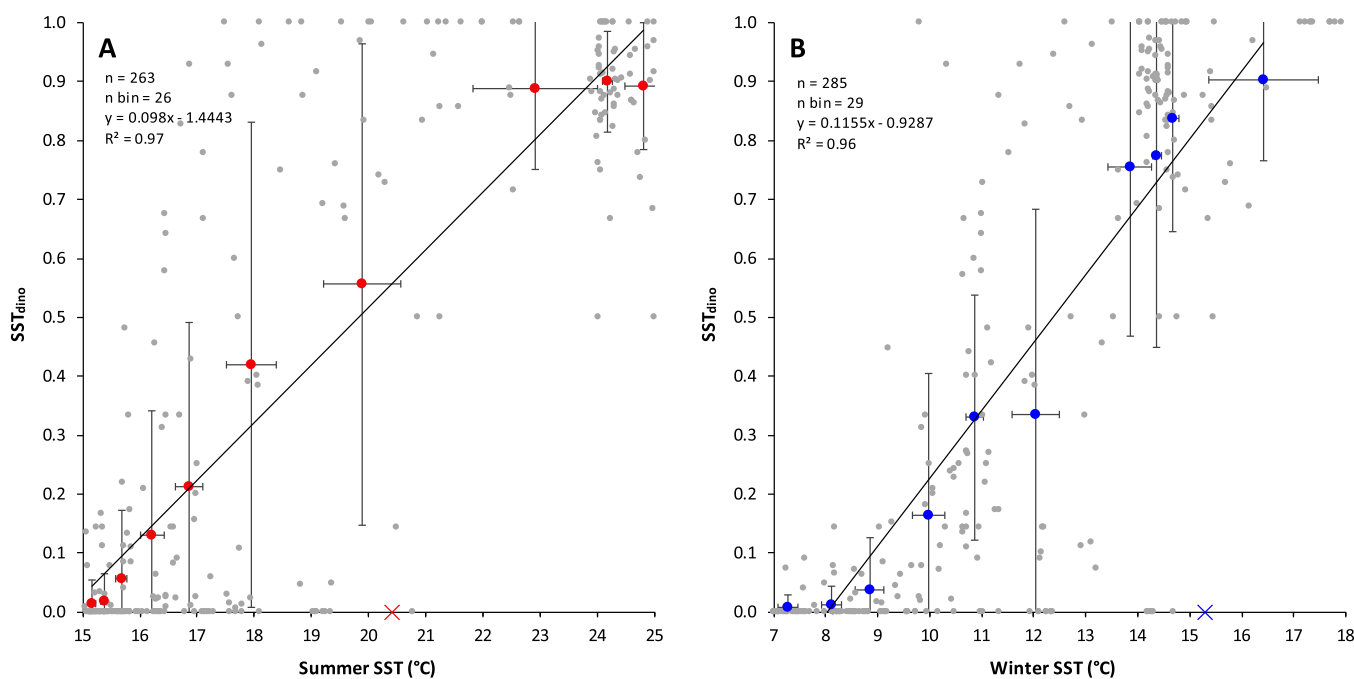

Fig. 3. Regression of SST_{dino} index versus present-day summer (A) and winter (B) SST. SST_{dino} was calculated on assemblages from the de Vernal et al. (2013a) dataset (in gray; see Appendix C1), which is available at http://www.geotop.ca/en/bases-de-donnees/dinokystes.html. The SST_{dino} and SST values (from the same sites) were averaged into 10 bins of equal size (red and blue) that were linearly regressed to emphasize the general trends (Section 3.4). Error bars indicate 1 standard deviation. Red and blue crosses indicate present-day summer and winter SST at the WIM (Section 2.1). (For interpretation of the references to color in this figure legend, the reader is referred to the web version of this article.)
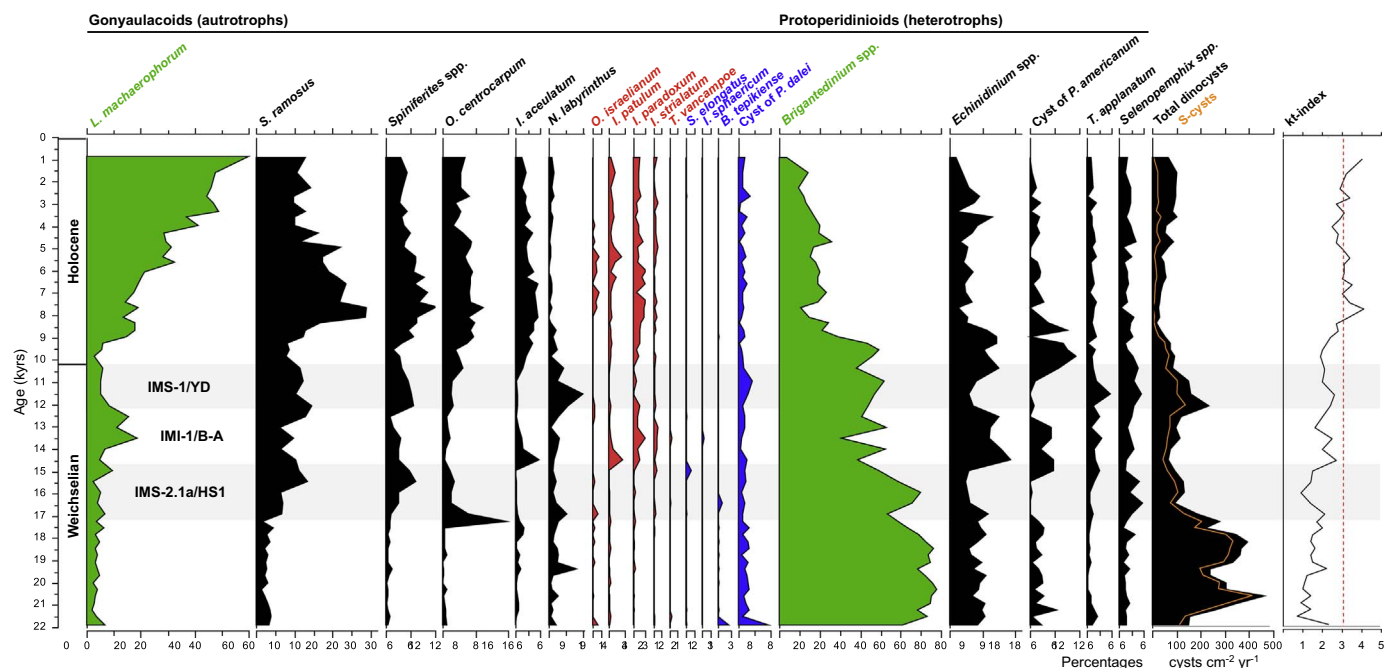
Fig. 4. Relative abundances of dinocyst taxa at Site U1385 over the last 22 kyr. All taxa that exceed 5% in one or more samples and all dinocyst taxa used in SST$_{dino}$ (Table 1) are included. Axes of *L. machaerophorum* and *Brigantedinium* spp. (green) are not in proportion to the axes of the other taxa, because these two taxa dominate assemblages. Dinocyst taxa used in SST$_{dino}$ are indicated in red (warm) and blue (cold). Some taxa have been grouped on genus level for the purpose of this plot (see Appendix A: Table A1 for a complete list of all taxa). *Brigantedinium* spp. includes *B. cariacoense*, *B. simplex* and *Brigantedinium* cysts that could not be identified on species level. *Echinidinium* spp. includes cf. cyst of *Oblea acanthocysta*, *E. aculeatum*, *Echinidinium* sp. A and *Echinidinium* sp. B cf. *E. delicatum*. *Spiniferites* spp. here includes all *Spiniferites* species, except *S. elongatus* and *S. ramosus*, which were plotted individually. *Selenopemphix* spp. includes *S. nephroides* and *S. quanta*. Dinocyst abundances are given in percentages; total dinocyst (black) and S-cyst (orange line) accumulation rates are in cysts cm^{-2} yr^{-1}. Red dashed line indicates a kt value of 3.1, above which degradation rates increase significantly (Section 3.4). Data are plotted on the age model of Hodell et al. (2015) (Section 3.2; Appendix B: Fig. B2). Gray shades represent IMS-1/YD and IMS-2.1a/HS1, as defined in Section 3.2. (For interpretation of the references to color in this figure legend, the reader is referred to the web version of this article.)

Xr = accumulation rate of R-cysts (cysts cm^{-2} yr^{-1}) and Xf = final accumulation rate of S-cysts (cysts cm^{-2} yr^{-1}) (Versteegh and Zonneveld, 2002; Zonneveld et al., 2007, 2008). When all S-cysts are preserved (Xi = Xf) kt = 0 and when all S-cysts are degraded the kt value increases to infinity. The relationship between kt and bottom water oxygen concentration is non-linear, with slowly increasing degradation rates up to a kt value of 3.1 and a shift to high degradation rates above this value (Zonneveld et al., 2007, 2008, 2010).

3.5. Quantitative SST, SSS and SSP reconstruction based on the modern analogue technique

We reconstruct variations in surface water parameters using the modern analogue technique (MAT) applied to dinocyst assemblages. The MAT is not a transfer function and as such does not rely on a mathematical relationship between taxa occurrences and sea-surface parameters, but simply assumes that similar assemblages are likely to occur under similar conditions (e.g. Guiot and de Vernal, 2007). Hence the MAT consists of 1) analyses of the similarity between modern and fossil assemblages by calculating the distance between the assemblages; 2) finding the five best analogues for the fossil assemblages in the modern dataset based on the shortest distance; 3) calculating paleo-surface water parameters based on a weighted average of the statistically significant modern analogues. The method, accuracy and limitations of the MAT are described in detail in de Vernal et al. (2001, 2005, 2013a, 2013b).

This study uses the updated standardized dinocyst database from the Northern Hemisphere that comprises 1492 surface samples from the North Atlantic, Arctic and North Pacific Oceans and their adjacent seas (e.g. Mediterranean Sea), as well as epicontinental environments (e.g. Estuary and Gulf of St. Lawrence, Bering Sea and Hudson Bay) (de Vernal et al., 2013a). The ranges of sea surface parameters in the

geographical and hydrographic domain of the n = 1492 database should be large enough for the reconstruction of glacial-interglacial sea-surface conditions at the study site (SST ~ -2–31 °C, SSS ~ 6–38, SSP ~ 10–660 gC m^{-2} yr^{-1}). However, the database mostly covers temperate to Arctic domains and the warm temperate and tropical environments are not very well represented ($\sim 15/8\%$ of the sites in the n = 1492 dataset have summer/winter SST values higher than at present-day WIM, Appendix C: Fig. C1), which may constitute a limitation for the reconstruction of warm interglacial conditions. Nomenclature and grouping of dinocyst taxa at Site U1385 conforms to the n = 1492 dataset. Taxa present in the fossil assemblages, but not in the modern dataset are excluded from the analyses for the application of MAT (*Dapsilidinium* spp., *Homotryblium* spp., *Melitasphaeridium* spp. and *Oblea acanthocysta*; maximum abundances of less than 1%). The search for the five closest analogues is made based on 54 taxa (see also Section 4.2.1).

For the application of MAT we use scripts prepared by Joël Guiot (CEREGE, France) for the software R (https://cran.r-project.org). The quality of the reconstruction is quantified based on the distance between the fossil and modern analogue assemblages (d) and the threshold distance value (d$_T$ = 1.37): analogues are good when d = 0 − d$_T$ / 2, acceptable when d = d$_T$ / 2 − d$_T$ and poor when d > d$_T$ (de Vernal et al., 2005; Appendix E: Table E1; Section 4.2.1). Only statistically significant analogues within the given threshold (d > d$_T$) are used, up to a number of five. We reconstruct seasonal (summer: July–September; winter: January–March) SST (°C) and SSS (unit less) and mean annual primary production, hereafter SST$_{MATsu}$, SST$_{MATwi}$, SSS$_{MAT}$ and SSP$_{MAT}$, respectively.

Validation exercises on MAT applied to the n = 1492 dataset, after log transformation of the data and search for the five best analogues, using the 54 taxa resulted in the following correlation coefficients (R^2) between observations and reconstructions: 0.96 and 0.98 for SST in summer and winter, 0.72 and 0.70 for SSS in summer and winter and

0.81 for SSP. Uncertainty estimates based on the errors of prediction were calculated from the standard deviation of the difference between observations and reconstructions. The errors of prediction are $\pm$ 1.63 °C and $\pm$ 1.14 °C for SST in summer and winter, $\pm$ 2.31 and $\pm$ 2.16 for SSS in summer and winter and $\pm$ 57 gC m^{-2} yr^{-1} for SSP.

4. Results

4.1. Qualitative paleoenvironmental reconstructions

A total of 56 dinocyst taxa have been identified (Appendix A: Table A1). Average Holocene and glacial stage dinocyst concentrations are ∼3800 and ∼7400 cysts per gram dry sediment, respectively, and mean accumulation rates are 62 and 217 cysts cm^{-2} yr^{-1}, respectively (Fig. 4). The degradation kt-index slowly increases towards ∼8 ka, yielding average values of 1.8 before and 3.2 and after ∼8 ka (Fig. 4). This implies increased impact of selective preservation on recorded assemblages towards the Holocene.

Brigantedinium spp. and *Lingulodinium machaerophorum* alternately dominate dinocyst assemblages throughout the record. Along with *L. machaerophorum*, *Spiniferites* spp. (mainly *S. ramosus*), *Operculodinium centrocarpum* and *Impagidinium* spp. (mainly *I. aculeatum*) dominate Holocene assemblages, while *Brigantedinium* spp. and *Echinidinium* spp. dominate the glacial stage (Fig. 4). *P. dalei*, *I. paradoxum* and *I. patulum* are the most abundant species included in the SST$_{dino}$ index. While *P. dalei* is more or less constantly present throughout the record, up to abundances of 7%, *I. paradoxum* and *I. patulum* are more abundant in

the Holocene and the B-A.

To test the quality of our empirical SST$_{dino}$ index, we calculated SST$_{dino}$ values on the modern assemblages dataset of de Vernal et al. (2013a) (for details see the text in Appendix C1). Regressions of SST$_{dino}$ with present-day sea surface parameters confirm that SST indeed dominantly drives the SST$_{dino}$ index, although with the present dataset we cannot exclude that a small part of the variation might also be related to SSS (Appendix C: Fig. C1). The downcore SST$_{dino}$ values clearly reflect glacial-interglacial, as well as stadial-interstadial variations (Fig. 5A), with minima of 0–0.1 in the glacial stage, HS1 and YD and maxima of 0.9–1 in the B-A and Holocene. Accumulation rates of R-cysts are relatively high in the glacial stage and at the beginning of the YD and lower in HS1, the B-A and the Holocene (Fig. 5F).

4.2. Quantitative reconstructions based on dinocysts

4.2.1. Quality of MAT reconstructions

When MAT was applied using all taxa in the assemblages, results were not optimal due to poor analogues. This is related to *Echinidinium* spp., *Protoperidinium americanum* and *Trinovantedinium applanatum*, which are abundant or common at Site U1385, but not sufficiently represented in the modern database. The representation of *Echinidinium* in the database might be questioned, because this taxon is difficult to identify at genus and species level (e.g. Radi et al., 2013). This is not the case for *P. americanum* and *T. applanatum* that are easy to identify. To circumvent this issue, we searched for analogues based on assemblages excluding *E. aculeatum*, *E. delicatum*, *Echinidinium* species only identified on genus level, *P. americanum* and *T. applanatum* in both the fossil
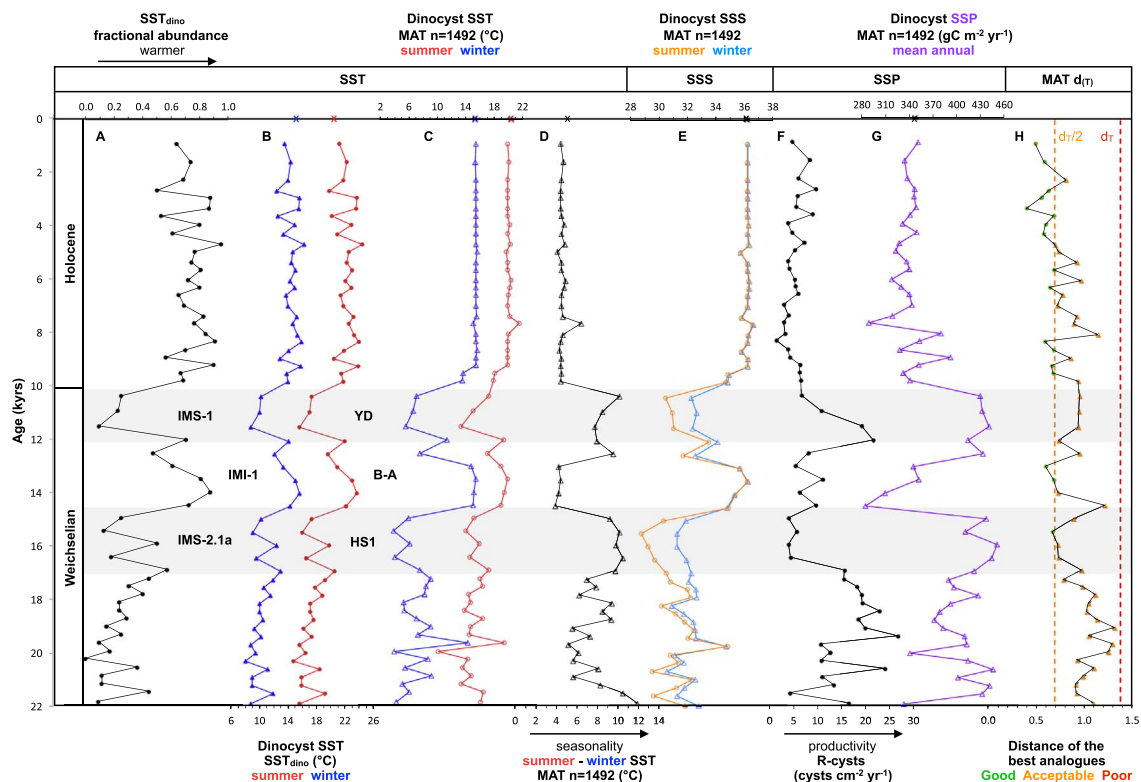

Fig. 5. Dinocyst-based climate records from Site U1385 encompassing the last glacial-interglacial transition and the Holocene. Data from Shackleton Site U1385, placed on the Hodell et al. (2015) time scale (Section 3.2; Appendix B: Fig. B2). (A) SST$_{dino}$ index of warm versus cold dinocysts (Section 3.4, Table 1). (B) Quantified SST$_{dino}$ index calculated from Fig. 5A and the regressions in Fig. 3 (Section 3.4). (C) Dinocyst MAT-based summer and winter SST (Section 3.5). (D) Difference between dinocyst MAT-based summer and winter SST (seasonality). (E) Dinocyst MAT-based summer and winter SSS (Section 3.5). (F) Accumulation rate of R-cysts (Section 3.4). (G) Dinocyst MAT-based mean annual primary production (Section 3.5). (H) Distances (d) between the fossil assemblages of samples of Site U1385 and their closest analogue in the modern n = 1492 database. Threshold distance value (d$_T$) = 1.144 (red dashed line). Analogues are good when d = 0–d$_T$ / 2 (green), acceptable when d = d$_T$ / 2 – d$_T$ (orange) and poor when d > d$_T$ (red) (de Vernal et al., 2005; Section 3.5). Alternating records are indicated with circles and triangles for convenience. Tracers based on indicator taxa and MAT are indicated with closed and open symbols, respectively. Crosses at 0 ka indicate present-day values. Gray shades represent IMS-1/YD and IMS-2.1a/HS1, as defined in Section 3.2. (For interpretation of the references to color in this figure legend, the reader is referred to the web version of this article.)

assemblages and modern database. In addition we grouped some *Spiniferites* species (*S. belerius*, *S. bulloideus*, *S. delicatus*, *S. lazus*, *S. pachydermus*, *S. membranaceus*, *Spiniferites* type granulaire) into *Spiniferites* spp.

The quality of MAT-based reconstructions relies on dinocyst concentrations and similarity of the encountered assemblages to samples in the modern analogue dataset. The minimum cyst accumulation rate encountered at Site U1385 for the last 22 kyr is 18 cysts $cm^{-2} yr^{-1}$, which is well above the threshold value of 1 cyst $cm^{-2} yr^{-1}$ (de Vernal et al., 2005). The similarity of the encountered assemblages to samples in the modern dataset is assessed through the reliability index (de Vernal et al., 2005). De Vernal et al. (2005) classified analogues to the modern dataset as 'good', 'acceptable' or 'poor' (Section 3.5). Using the grouping of species as described above, we obtained analogues for all 56 samples (Appendix E: Table E1, Fig. 5H). The dinocyst assemblages in the n = 1492 dataset are similar to the glacial-interglacial assemblages at Site U1385 to such a degree that the closest analogue scored 'good' for 17 samples and 'acceptable' for 39 samples. Only some of the fifth analogues scored 'poor', hence MAT-based reconstructions are based on all five analogues for most samples.

Of the 1492 sites of the de Vernal et al. (2013a) dataset 45 unique sites were chosen as analogues for samples of Site U1385 (Appendix C: Fig. C2; Appendix E: Table E1). Most analogues are from the southern WIM, the western Mediterranean Sea, along the coast of Norway and from along the east and west coasts of the USA (Appendix C: Fig. C2). Site A265 from the southern WIM (~65 km northeast of Site U1385, very close to Site SO75-6KL (Boessenkool et al., 2001; Figs. 1 and C2) is most used as analogue (16% of all selected analogues). For the Holocene and B-A most analogues (~80%) are from the southern WIM and the Mediterranean Sea and Site A265 is the only site selected as best (first) analogue. For the YD, HS1 and the glacial stage Site A265 is still among the top three most used analogues, although for these colder periods more sites (50%) from colder regions (both coasts of the USA and along the coast of Norway) are selected.

4.2.2. Sea surface temperature, salinity and production

Generally, SST_{MAT} and the qualitative and quantified SST_{dino} give similar results, with relatively low temperatures in the glacial, HS1 and the YD and high temperatures in the B-A and Holocene (Fig. 5A–C). SST_{MATwi} and SST_{dino} show the stadial and interstadial phases somewhat clearer than SST_{MATsu} and the quantified index, which show less amplitude. The smaller amplitude changes of the quantified index are the result of the limited range of SSTs that can be reconstructed with the regression (Section 3.4) compared to SST_{MATwi} (Section 3.5). However, SST_{MATsu} shows changes of similar amplitude as the quantified index, although the possible range of reconstruction is similar for summer and winter MAT (Section 3.5). The variable Holocene in SST_{dino} contrasts with the very flat SST_{MAT} record and SST_{dinosu} is on average 2.4 °C higher than SST_{MATsu} over the entire 22 kyr. The highest SSTs that are reconstructed with MAT are 19.9 °C and 15.3 °C for summer and winter respectively (Holocene averages, Fig. 5C), which are the same as present-day SST_{su} and SST_{wi} along the WIM (Section 2.1) considering the errors of prediction of the MAT (Section 3.5). These SSTs constitute an upper SST limit for the MAT approach, while no lower limit is apparent. This is further illustrated by linear regressions of the qualitative and quantified index with MAT (Fig. 6A–B), which show significant correlation with SST_{MAT} up to this upper MAT limit. SST_{dinowi} reconstructs SSTs 3.4 °C higher (on average) than SST_{MATwi} for the YD, HS1 and the glacial stage, which is related to the lower limit (of 8.04 °C) of the quantified index. SST_{MATwi} reconstructs similar SSTs as SST_{dinowi} for the Holocene and B-A (14.9 °C and 14.4 °C on average, respectively) despite the upper limit of the MAT.

In the glacial stage, before the B-A, SST_{MATsu} is relatively and continuously high, with summer temperatures averaging 15.0 °C, 5.4 °C colder than present, while winter temperatures average 6.9 °C, 8.4 °C colder than present. Variability in seasonality is, hence, dominantly

determined by SST_{MATwi} and shows distinct maxima in the glacial stage (~22 ka), HS1 and the YD, ~4 °C higher than in the Holocene (Fig. 5C). The data suggests seasonality similar to the present day during some parts of the glacial stage, the B-A and the Holocene. Regressions of SST_{dino} versus summer and winter SST have a similar slope (Fig. 3), hence no (substantial) changes in seasonality are reconstructed with the quantified index.

SSS_{MATsu} and SSS_{MATwi} are very similar throughout the record and are generally ~4.5 lower in the glacial stage than in the Holocene (Fig. 5E). SSS_{MATsu} decreases 1–2 units more than SSS_{MATwi} in HS1 (to ~29.7) and the YD (to ~31.5), while SSS_{MATsu} and SSS_{MATwi} are similarly high and reach values similar to the Holocene in the B-A. The SSS_{MAT} record closely follows the trend in SST_{MATwi} and hence also resembles SST_{dino} (Fig. 6C). In the Holocene, SSS_{MAT} is very stable and averages 36.2, which is the same as present-day SSS along the WIM considering the errors of prediction of the MAT and also constitutes an upper SSS limit for the MAT (Fig. 6C; Sections 2.1 and 3.5). For both SST and SSS all values above the limits (Fig. 6) are from the Holocene and B-A.

Mean annual primary production as reconstructed from MAT (SSP_{MAT}) is generally high in the glacial, HS1 and the YD, averaging 409 gC $m^{-2} yr^{-1}$ (Fig. 5G). SSP_{MAT} drops to 283 gC $m^{-2} yr^{-1}$ during the B-A and decreases after the YD to an average of 339 gC $m^{-2} yr^{-1}$ in the Holocene, similar to present-day SSP along the WIM (Section 2.1).

5. Discussion

5.1. Pentapharsodinium dalei as cold-water indicator

The cyst of *Pentapharsodinium dalei* is abundant in subarctic environments (e.g. de Vernal et al., 2013a) and may represent an important environmental indicator. We therefore use this species in our SST_{dino} index (Table 1; Fig. 5A), where it is the most abundant cold-water indicator (Fig. 4). Strikingly, the occurrence of this species has not been consistently reported along the WIM, either in studies dealing with modern dinocyst assemblages (Sprangers et al., 2004, transects along the WIM; Ribeiro and Amorim, 2008, Lisbon Bay) or the last glacial transition (Boessenkool et al., 2001, Site SO75-6KL). However, other authors have found *P. dalei* in sediments of Sites SU81-18 and MD95-2042 for the entire last glacial cycle (MIS1-6; Turon et al., 2003; Eynaud, 1999, Eynaud et al., 2000; Sanchez Goñi et al., 1999, 2000a, 2000b, 2002, 2008; Penaud et al., 2011a) and at Site U1385 for MIS11 and MIS19 (Eynaud et al., 2016). The cyst of *P. dalei* might have been overlooked in some previous dinocyst studies, possibly due to the small size (19–36 μm; cf. Rochon et al., 1999) and/or thin and colorless wall. Alternatively, *P. dalei* may have been lost when the samples were sieved with mesh size larger than 10 μm (e.g. Ribeiro and Amorim, 2008; Lignum et al., 2008).

5.2. Comparison of the quantified index and MAT: limits and advantages of both methods

SST and SSS reconstructed with the MAT are limited at present-day values (Section 4.2.2, Figs. 5 and 6). It is possible to reconstruct SSTs and SSSs above these values with MAT, because the n = 1492 reference dataset (de Vernal et al., 2013a) includes sufficient sites with SSTs and SSSs well above these limits. However, the number of these > limit sites in n = 1492 is relatively small compared to the < limit sites (Section 3.5), which hinders the reconstruction of warm interglacial conditions.

The sites from the n = 1492 dataset used for samples beyond this limit are not from a single region, but come from the southern WIM, Mediterranean Sea, off Morocco, the Gulf of Biscay, off the Delmarva Peninsula (East coast USA) and from along the coast of Mexico. Dinocyst assemblages at all these sites are sufficiently different from the downcore Site U1385 assemblages that they were hardly ever selected
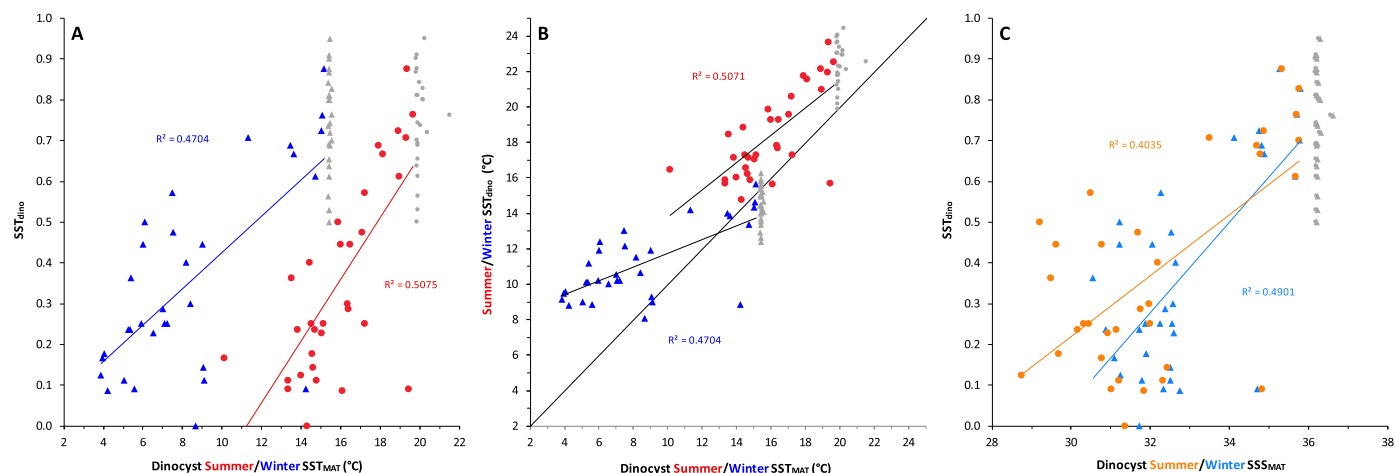
Fig. 6. Linear regressions of (A) SST_{dino} versus SST_{MAT}, (B) quantified SST_{dino} versus SST_{MAT} and (C) SST_{dino} versus SSS_{MAT} calculated on fossil assemblages of Site U1385. Data can be found in Table A1 and Table E1. Red/orange circles represent summer values; blue triangles represent winter values. MAT results show samples with > limit values (gray) for SST_{MATsu}, SST_{MATwi} and SSS_{MAT} at 19.8 °C, 15.35 °C and 36.1, respectively, which are hence excluded from regressions. (For interpretation of the references to color in this figure legend, the reader is referred to the web version of this article.)

as analogues in the MAT analyses. Less than 0.5% of the analogues that were selected for Site U1385 from the n = 1492 dataset have SST and SSS values above the limits seen in Fig. 6. If selected, they were far more often second to fifth analogue than first. The sites with the highest SSTs and SSSs that have assemblages that are relatively similar to those from Site U1385 are from the WIM itself (mainly Site A265, Appendix C: Fig. C2), hence the limit at present-day values.

The larger number of sites in the n = 1492 dataset with low values for SST and SSS results in ample analogues for the colder periods (YD, HS1 and glacial stage). Still, 50% of the analogues selected for these cold periods are from the WIM (and Mediterranean Sea), suggesting that dinocyst assemblages are also influenced by site-specific parameters that are not acknowledged in the model. Moreover, the MAT calculates similarity based on entire assemblages and not specific selected warm/cold taxa only. Sites closest to the study site can hence have the most similar assemblages, even though the sea surface parameters related to downcore assemblages may be more similar to sites from different regions in the n = 1492 dataset. This may influence the MAT for some samples, although the MAT works well for most samples. Notably, several sites from along the WIM were never chosen as analogues for our downcore assemblages, despite their proximity to Site U1385 (Appendix C: Fig. C2 inset). The other 50% of the analogues selected for the YD, HS1 and glacial stage are from the east and west coasts of the USA, North and Norwegian Seas, Iceland and the Northwestern Passages (Appendix C: Fig. C2). Apparently these colder analogues sufficiently contribute to the reconstruction of lower SSTs, because no lower limit in MAT is observed.

The quantified index also has limitations. The exact SST values that are assigned to the qualitative index not only depend on the observed relation between the qualitative index and present-day SST (Appendix C: Fig. C1B–C), but also on the type of regression used (linear), the chosen amount of data bins (10) and the exact interval chosen for the calculation of the regression (Fig. 3). In addition, the scatter in index values is quite large (Fig. 3). Hence, the quantified index merely serves as a general SST indicator and should not be overinterpreted. Also, the taxa used in the dinocyst index are 'warm' and 'cold' indicators relative to present-day SSTs locally at Site U1385 (Section 2.1) and not relative to the North Atlantic as a whole. Since the largest part of the n = 1492 dataset (de Vernal et al., 2013a) is 'cold' relative to the present-day WIM, a lower limit of the quantified index, where the index remains 0 for continuingly decreasing SSTs, was expected. Only a small part of the n = 1492 dataset is 'warm' relative to the present-day WIM and from Appendix C: Fig. C1B–C it seems that an upper limit for the quantified

index is not yet reached with this reference dataset. However, Fig. 3 shows that there is a possible upper limit at ~24 °C for SST_{dinosu}. Due to the local character of the qualitative index only a certain range of SSTs can be reconstructed (Section 3.4, Appendix C). Beyond the minimum and maximum SSTs that can be reconstructed, SSTs continue to de/increase, but the qualitative index remains 0/1. Hence, the minimum and maximum summer and winter SSTs should be interpreted as 14.74 °C and 8.04 °C or lower and 24.94 °C and 16.70 °C or higher.

Both the MAT method and the quantified index were applied to the same reference dataset of (de Vernal et al., 2013a), hence observed differences in reconstructed SSTs (Section 5.3) are related to the difference in both methods. The MAT reconstructs more reliable SSTs, with a much smaller error of prediction than the quantified index, but only up to present-day WIM values. The quantified index also has a limited range of SSTs that can be reconstructed (especially for the lower SSTs), but it can reconstruct $SST_{(su)}$ beyond the upper limit of the MAT. Hence the methods are complementary: MAT can be used for reconstructions in the colder periods (YD, HS1 and glacial stage), with a small error of prediction and the quantified index can be used to estimate SST beyond the limit of the MAT (Holocene and B-A), though with much less precision.

5.3. Sea surface temperature

5.3.1. Holocene temperature variability

In the Holocene, SST_{MAT} variability is much lower than that of SST_{dino} (Fig. 5A–C). The SST_{dino} index at sites SO75-6KL and SU81-18 for the same interval is also highly variable (Boessenkool et al., 2001; Eynaud et al., 2016, Fig. 7D), while foraminiferal $\delta^{18}O$ from sites U1385, MD01-2444 and MD95-2042 (e.g. Hodell et al., 2013b, Fig. 7B; Salgueiro et al., 2014; Hodell et al., 2015, Fig. 7C), $U_{37}^{k'}$ from sites MD01-2444 and MD95-2042 (e.g. Pailler and Bard, 2002; Martrat et al., 2007; Darfeuil et al., 2016, Fig. 7E–F) and MAT estimates based on dinocyst and foraminiferal census counts from sites MD95-2040/41/42 and SU81-18 (Penaud et al., 2011b; Voelker and Abreu, 2011; Salgueiro et al., 2014, Fig. 7G–H) show more stable Holocene SSTs. This is quite peculiar because it was previously shown from many different proxy records that the climate of the Holocene in the North Atlantic region was not stable and punctuated by abrupt shifts of large amplitude (e.g. Bond et al., 1997, 1999; Mayewski et al., 2004).

For the MAT, the limited number of analogues for the 'Warm Ocean' (Section 3.5) contributes to low sensitivity of SST_{MAT} (Section 5.2). The fundamental difference in the way the biogenic tracers are used to
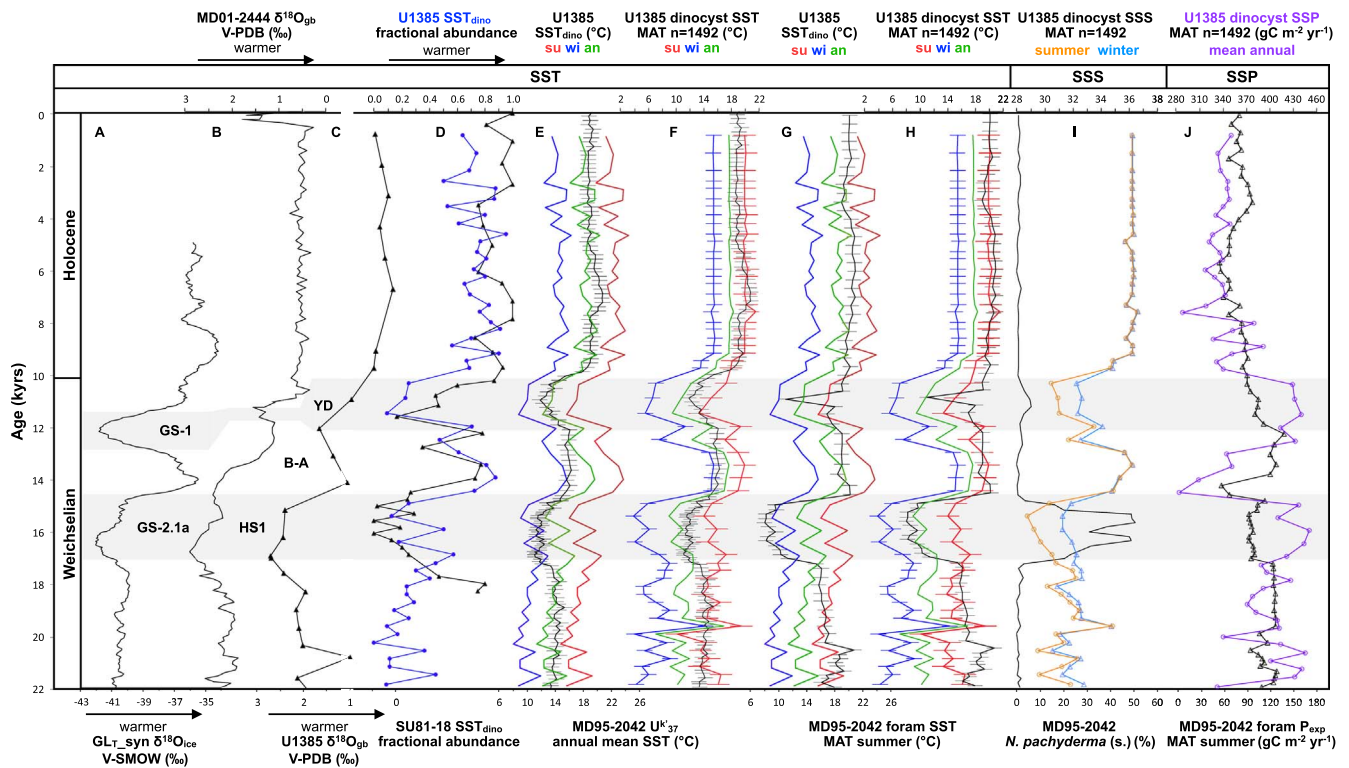
Fig. 7. Climate records from the Greenland ice core and West Iberian Margin marine cores for the last 22 kyr. Colored records indicate data of Site U1385 (this study, see legend of Fig. 5), black records indicate previously published records (Greenland ice core and Sites MD95-2042/SU81-18). Data from Shackleton Site U1385 are placed on the Hodell et al. (2015) time scale (Section 3.2; Appendix B: Fig. B2), to which we aligned Sites MD95-2042 (using the age model of Darfeuil et al., 2016) and SU81-18 (using the age model of Bard et al., 2000). (A) Greenland synthetic $\delta^{18}O$ temperature record of Barker et al. (2011) placed on Speleo-Age (Section 3.2). (B) Planktic foraminifer (*G. bulloides*) $\delta^{18}O$ from Site MD01-2444 (Hodell et al., 2013b) placed on the Hodell et al. (2013b) time scale (Section 3.2). (C) Planktic foraminifer (*G. bulloides*) $\delta^{18}O$ of Site U1385 (Hodell et al., 2015). (D) SST_{dino} index as defined in this study (Table 1, Section 3.4) calculated on dinocyst assemblages of Site SU81-18 (Eynaud et al., 2016). (E–F) Quantified index and dinocyst MAT-based SST of Site U1385, including averaged summer and winter SSTs to represent mean annual dinocyst SST (green) and $U^{k'}_{37}$ of Site MD95-2042 calculated using the calibration of Conte et al. (2006) (Darfeuil et al., 2016). (G–H) Foraminiferal MAT-based summer SST of Site MD95-2042 (Salgueiro et al., 2014). (I) Relative abundances of *Neogloboquadrina pachyderma* (s.) of Site MD95-2042 (Salgueiro et al., 2014). (J) Foraminifer MAT-based summer export production of Site MD95-2042 (Salgueiro et al., 2014). Gray shades represent GS-1/YD and GS-2.1a/HS1, as defined in Section 3.2. Note that the Holocene is defined as the end of GS-1/YD, and is hence not fixed at a certain age in this figure. (For interpretation of the references to color in this figure legend, the reader is referred to the web version of this article.)

estimate temperature might also contribute to the dissimilarities. SST_{dino} is a fractional abundance based only on a selection of 'warm' and 'cold' dinocysts, while SST_{MAT} is a quantitative approach considering the overall assemblages. Using only a small part of the assemblage (Table 1), SST_{dino} potentially allows for more variability as the dampening effect of a large assemblage is excluded. It is also possible that the taxa used for the index do not react exclusively to temperature and capture another parameter, although the dataset of modern assemblages (de Vernal et al., 2013a) shows that SST is the dominant factor determining SST_{dino} (Appendix C1; Fig. C1). Also for the MAT a parameter other than SST might play a role, since the MAT reconstructs SST based on similarity of complete assemblages and not warm/cold taxa only. With regard to alkenones and foraminifers, shifts in the blooming season or depth habitat to maintain optimal metabolic activities might also result in attenuated temperature signals.

5.3.2. Comparison between the glacial stage and the Holocene

SST_{MATsu} and SST_{dinosu} indicate relatively warm glacial summer temperatures averaging ~15.0 °C and ~17.1 °C, compared to ~20.0 °C and ~22.3 °C for the Holocene, respectively (Fig. 5B–C). For SST_{dinosu} the relatively high glacial SSTs might be related to the limited range in SSTs that can be reconstructed with the regression, however the MAT, which is not bound by a lower limit, reconstructs similar high glacial summer SSTs. Also, the reconstructed Holocene and glacial SST_{MATsu} and SST_{dinosu} are consistent with previous quantifications from dinocyst MAT (de Vernal et al., 2005), $U^{k'}_{37}$ (Pailler and Bard, 2002; Martrat et al., 2007; Darfeuil et al., 2016, Fig. 7E–F), and foraminiferal MAT

(Penaud et al., 2011b; Voelker and de Abreu, 2011; Salgueiro et al., 2014, Fig. 7G–H) at nearby sites MD01-2444, MD95-2040/41/42 and SU81-18 that also show glacial (summer) SSTs ~5 °C lower than in the Holocene. Penaud et al. (2011b) have previously performed MAT analyses on dinocyst assemblages from Site SU81-18 over the last 30 kyr using the reference dataset of Radi and de Vernal (2008) with 1189 samples. Their R-1189 dinocyst SST_{MATaug} shows two data points with much lower glacial summer SSTs (~2 °C) compared to our SST_{MATsu} and SST_{dinosu}, but also one data point that is several degrees higher. However, Penaud et al. (2011b) were not able to find analogues for most of their samples and their reconstruction is based on a few discontinuous data points only.

Our Holocene SST_{MATwi} value of 15.4 °C matches the modern SST_{wi} at ~15.3 °C (Fig. 5C; World Ocean Database: Boyer et al., 2013), but this is also close to the upper limit of the MAT (Section 5.2). However, SST_{dinowi} and previous quantifications from foraminiferal MAT (Penaud et al., 2011b; Voelker and de Abreu, 2011) at nearby sites MD95-2041 and SU81-18 reconstruct similar Holocene winter SSTs (14.5 °C and ~15–16 °C, respectively) considering the errors of prediction, suggesting that SST_{MATwi} provides reliable winter temperatures.

In contrast to SST_{MATsu}, our SST_{MATwi} indicates a relatively cold glacial stage (averaging ~7.3 °C), ~8.1 °C lower than in the Holocene. The relatively high SST_{dinowi} values suggesting high glacial winter SSTs (~10 °C) are related to the lower limit of the quantified index (Section 5.2). De Vernal et al. (2005) also quantify a slightly warmer glacial dinocyst SST_{MATwi} of 8.9 °C at site SU81-18, but this work used an older (n = 940) reference modern database. Our new results of Site U1385,

based on n = 1492, are statistically more sound. Dinocyst SST_{MATfeb} from Site SU81-18 (R-1189 reconstruction, Penaud et al., 2011b) shows relatively cold conditions during the glacial stage (~ -1 °C), although much lower than our SST_{MATwi}, but indicates quite warm glacial winter SSTs (~ 18 °C) just before HS1, in contrast to our results. However, this comparison is again based on only a few discontinuous data points that are based on the older n = 1189 reference dataset. Foraminiferal SST_{MATwi} at sites SU81-18 and MD95-2040/41 indicate glacial SSTs of $\sim 11–12$ °C, also warmer than our SST_{MATwi} and SST_{dinowi} and hence, only ~ 5 °C lower than in the Holocene, similar to the SST_{MATsu} signal (Penaud et al., 2011b; Voelker and de Abreu, 2011). At nearby Site MD95-2042, Penaud et al. (2011a) reconstructed February and winter SSTs of ~ 10 °C based on a MAT approach of dinocysts and planktonic foraminifers, between 50 and 25 kyr. Our somewhat lower values would be consistent with a general cooling trend towards the LGM.

Our qualitative SST_{dino} index also indicates a relatively cold glacial stage in contrast to relative SSTs based on warm/cold dinocyst species from Site SO75-6KL (Boessenkool et al., 2001) that indicate a relatively warm glacial stage with SSTs similar to the Holocene. However, this could possibly be related to the absence of *P. dalei* in their assemblages. Although foraminiferal $\delta^{18}O$ records from sites U1385, MD01-2444, MD95-2042 and SU81-18 indicate a glacial stage that was relatively warm compared to the surrounding HSs, HS1 is not much cooler than the glacial and foraminiferal $\delta^{18}O$ show a relatively cool glacial stage when compared to the Holocene, in agreement with our SST_{dino} index (Cayre et al., 1999; Shackleton et al., 2000; Eynaud et al., 2009; Hodell et al., 2013b, Fig. 7B; Hodell et al., 2015, Fig. 7C; Salgueiro et al., 2014; Govin et al., 2014).

De Vernal et al. (2006) previously showed that reconstructed glacial SSTs could significantly differ depending on the tracers used. Here we show that the quantitative tracers based on dinocysts, alkenones and foraminifera agree on a relatively warm glacial summer, only a few degrees colder than in the Holocene. However, reconstructions for glacial winter SSTs diverge more between the different dinoflagellate and foraminiferal tracers. Our MAT results indicate a colder glacial winter than previously reconstructed.

5.3.3. Seasonality

Holocene seasonality based on the difference between SST_{MATsu} and SST_{MATwi} at Site U1385 is ~ 4.6 °C, very similar to the present day seasonal SST difference at the WIM (5.1 °C, World Ocean Database: Boyer et al., 2013), although this might be related to the limits of the MAT (Section 5.2). However, previous quantifications from foraminiferal MAT (Penaud et al., 2011b; Voelker and de Abreu, 2011) at nearby sites MD95-2041 and SU81-18 reconstruct similar Holocene seasonality (~ 5 °C and ~ 4.4 °C, respectively), suggesting that seasonality in the Holocene indeed was similar to today.

SST_{MAT} suggests that seasonality was higher during the glacial stage, HS1 and the YD (~ 8.3 °C), due to relatively cold winters (Fig. 5D). These results agree with dinocyst-based SST_{MAT} reconstructions of de Vernal et al. (2000, 2005) who show that along the continental margin of Europe on the whole, SST anomalies between LGM and present-day are more negative in winter than in summer. In contrast, previous quantifications from foraminiferal MAT (Penaud et al., 2011b; Voelker and de Abreu, 2011) at nearby sites MD95-2041 and SU81-18 reconstruct glacial seasonality similar to the Holocene (~ 5 °C and ~ 4.7 °C, respectively). Seasonality based on the quantified index is constant (~ 7.5 °C) over the entire studied interval, but this is related to the similar slopes of the summer and winter regressions (Fig. 3) and hence might represent an artifact.

Penaud et al. (2011a) reconstruct seasonal contrasts similar to our MAT using dinocyst- and planktonic foraminiferal-based reconstructions at Site MD95-2042 for the glacial interval between 50 and 25 kyr. The larger seasonal SST contrast of the glacial stage could be related to increased freshwater discharge (Section 5.4). Lower SSS (Fig. 5E) and a resulting buoyant, shallow, low-density surface water layer would

result in a low thermal inertia in the surface waters that could explain the large amplitude changes from winter to summer (de Vernal et al., 2000, 2005).

5.3.4. Stadial-interstadial variability

It was previously demonstrated that the millennial-scale climate variability at the Shackleton Site could be correlated to the Greenland ice core records using e.g. oxygen isotope variability in planktonic foraminifera (e.g. Shackleton et al., 2000). SST_{dino} and SST_{MAT} clearly reflect HS1, the B-A and the YD at Site U1385 and match the Greenland (inter)stadials, with an even stronger signal than the planktonic foraminiferal $\delta^{18}O$ at sites U1385 and MD01-2444 (Fig. 7A–F). Hence correlation is also possible based on qualitative and quantitative temperatures derived from dinocysts.

SST_{dino}, the quantified SST_{dino} and SST_{MAT} also generally agree with HS1, the B-A and the YD, as previously recognized in many records based on dinocysts (Boessenkool et al., 2001; Eynaud et al., 2016, Fig. 7D), alkenones (Bard et al., 2000; Pailler and Bard, 2002; Martrat et al., 2007; Darfeuil et al., 2016, Fig. 7E–F) and foraminifers (Cayre et al., 1999; Shackleton et al., 2000; Eynaud et al., 2009; Penaud et al., 2011b; Voelker and Abreu, 2011; Hodell et al., 2013b; Salgueiro et al., 2014, Fig. 7G–H; Govin et al., 2014; Hodell et al., 2015, Fig. 7C) from sites along the WIM (SO75-6KL, SU81-18, MD01-2444, MD95-2040/41/42, U1385). However, we observe some differences between SST_{dino}, the quantified SST_{dino} and SST_{MAT} and between dinocyst-based SST estimates and alkenone and foraminiferal-based estimates, as further discussed in the sections below.

5.3.5. Comparison between dinocyst SST and $U^{k'}_{37}$

Absolute summer SST_{MAT} values as well as amplitude variations are quite similar to $U^{k'}_{37}$ from sites MD01-2444 and MD95-2042, especially for the Holocene and the Glacial stage, while they are slightly higher than $U^{k'}_{37}$ in the YD, B-A and HS1 (Pailler and Bard, 2002; Martrat et al., 2007; Darfeuil et al., 2016, Fig. 7F). Regression of SST_{MATsu} versus $U^{k'}_{37}$-based SSTs of Darfeuil et al. (2016) (Fig. 8A) confirms that the two tracers give similar results with a regression line close to, but slightly above the 1:1 line (Fig. 8A). SST_{MATwi} is significantly lower than the $U^{k'}_{37}$-based SST (Fig. 7F, Fig. 8A), beyond tracer uncertainty (Section 3.5; Müller et al., 1998) over the entire studied interval, except during the B-A. SST_{MAT} and $U^{k'}_{37}$ are well correlated until the SST_{MAT} limit value (Fig. 8A). This is the same limit as in the regression of SST_{MAT} versus the index (Fig. 6A) confirming the limitation of the MAT method.

$U^{k'}_{37}$ is not skewed to summer or winter SST_{dino} for the Holocene, the YD and the glacial stage, but is more similar to SST_{dinowi} for the B-A and HS1 (Fig. 7E). Regression of the quantified SST_{dino} index versus $U^{k'}_{37}$ shows the very stable Holocene (~ 19 °C) and Glacial stage (~ 14 °C) of $U^{k'}_{37}$ where the quantified index is more variable (Fig. 8B). The regression confirms that in general over the 22 kyr $U^{k'}_{37}$ is not skewed to summer or winter SST_{dino}. We averaged summer and winter SSTs for both dinocyst methods, to represent mean annual dinocyst SST and regress it versus $U^{k'}_{37}$ (Fig. 8C). Mean annual SST of the quantified index is similar to $U^{k'}_{37}$, while SST_{MATan} reconstructs slightly lower average SSTs compared to $U^{k'}_{37}$ (Figs. 7E–F & 8C).

Previous studies in this area have assumed that $U^{k'}_{37}$ reflects mean annual SSTs (e.g. Bard et al., 2000; Bard, 2001; Pailler and Bard, 2002; Martrat et al., 2007; Rodrigues et al., 2011). Also, in contrast to our results from Site U1385, alkenone-based SST reconstructions are closer to dinocyst SST_{MATfeb} than to SST_{MATaug} at a site off Morocco during the glacial, HS1 and the YD (Penaud et al., 2010, 2011b) and at Site MD95-2042 between 50 and 25 kyr (Penaud et al., 2011a). If $U^{k'}_{37}$ indeed reflects mean annual SSTs, or even winter SSTs during colder periods, this implies that (the warmer) SSTs reconstructed with the quantified index are more accurate than reconstructions from the MAT, which would slightly underrepresent $SST_{(su)}$.

In contrast, de Vernal et al. (2006) and Darfeuil et al. (2016) hinted that the $U^{k'}_{37}$-based SST signal does not fully reflect mean annual
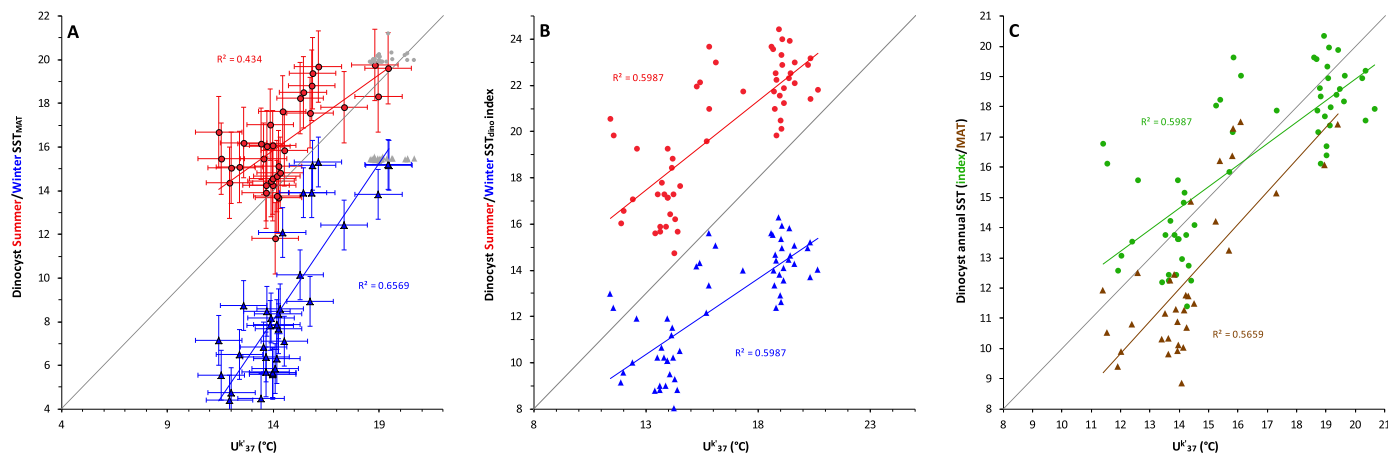
Fig. 8. Linear regressions of (A) SST$_{MAT}$ and (B) quantified SST$_{dino}$ calculated on fossil assemblages of Site U1385 versus U$^{k'}_{37}$ of Site MD95-2042 (Darfeuil et al., 2016). Samples with > limit values for MAT (gray) were excluded from regressions. We used the U$^{k'}_{37}$ of Site MD95-2042 calculated using the calibration of Conte et al. (2006) (Darfeuil et al., 2016), placed on the age model of Darfeuil et al. (2016) and aligned ages to Site U1385. We resampled the U$^{k'}_{37}$ record to the age scale of U1385 using Analyseries and calculated a linear regression between the two datasets. Error bars indicate errors of prediction of SST$_{MAT}$ (Section 3.5) and U$^{k'}_{37}$ (Darfeuil et al., 2016). Red circles represent summer SST; blue triangles represent winter SST. Averaged summer and winter SSTs (C) represent mean annual dinocyst SST for the quantified index (green circles) and MAT (brown triangles). (For interpretation of the references to color in this figure legend, the reader is referred to the web version of this article.)

temperature and might be skewed towards summer SSTs in the study region for glacial times. Also, remotely sensed particulate inorganic carbon (PIC) and chlorophyll data indicate that the alkenone producer *Emiliania huxleyi* mainly blooms in spring to early summer along the WIM (Hopkins et al., 2015). This implies that SST$_{MAT}$ would reconstruct more accurate SST$_{(su)}$ and that the quantified index would over represent SST$_{(su)}$. With the present data it is difficult to draw a conclusion about the accuracy of both dinocyst methods.

The combined information suggests that the seasonality reflected in the tracers may differ between sites and over time. Local and temporal changes in upwelling intensity along the WIM and related changes in stratification of the water column might affect the taxa differently. Therefore, the differences in recorded SSTs could be due to shifts in timing of the maximum production of the different taxa over time (Sangiorgi et al., 2003; Voelker and de Abreu, 2011).

5.3.6. Comparison between dinocyst SST and foraminiferal MAT

For HS1, planktic foraminifer-based SST$_{MATsu}$ of nearby sites MD95-2041/42 and SU81-18 are several degrees cooler than our dinocyst based SST$_{MATsu}$ and even more similar to SST$_{dinowi}$ than SST$_{dinosu}$, while dinocyst and foraminiferal SST$_{MATwi}$ are similar (Penaud et al., 2011b; Voelker and Abreu, 2011; Salgueiro et al., 2014, Fig. 7G–H). For the B-A and the YD, both the summer and winter foraminiferal SST$_{MAT}$ of sites MD95-2042 and SU81-18 are very similar to the temperatures indicated by the dinocyst SST$_{MAT}$ (Penaud et al., 2011b; Salgueiro et al., 2014, Fig. 7G–H). For the B-A, foraminifer-based SST$_{MATsu}$ is more similar to average (annual) summer-winter SST$_{dino}$ than to SST$_{dinosu}$. Interestingly, the YD does not stand out in the foraminifer-based SST$_{MAT}$ of nearby sites MD95-2041/42 and the more northern sites MD95-2040 and SU92-03 (Salgueiro et al., 2010; Voelker and Abreu, 2011), even though these records have sufficient temporal resolution and there is sufficient coverage of the modern foraminifer database in terms of diversity of taxa and SST range (Kucera et al., 2005). The differences between dinocyst and foraminiferal MAT-based SST estimates are well beyond the uncertainty of the respective approaches. Although the MAT works in a similar way for foraminifera and dinocysts, the methods are not exactly the same (e.g. different reference database and software), hence differences in the method could cause differences in reconstructed SSTs. An ecological bias could also cause the observed differences. Several authors state that different SST signatures from dinocysts and foraminifera could be related to differences in depth habitat; dinoflagellates live in the surface ocean, while some

foraminiferal species migrate to deeper parts of the water column during their life cycle (e.g. de Vernal et al., 2005, 2006; Penaud et al., 2011a, 2011b). This is particularly critical considering that the thermal structure of the upper ocean may have changed through time (Telford et al., 2013).

5.4. Sea surface salinity

The stable Holocene SSS$_{MATdino}$, with an average value of 36.2, corresponds to the present-day SSS value and absence of seasonality along the WIM (SSS$_{su}$ and SSS$_{wi}$ = 36.1, World Ocean Database: Boyer et al., 2013; Fig. 5E). It should be noted, however, that this value represents the upper limit of the MAT (Section 5.2). The generally lower glacial SSS$_{MAT}$ (beyond tracer uncertainty) is consistent with SSS$_{MAT}$ reconstructions of de Vernal et al. (2000, 2005) who show that LGM SSS in the North Atlantic and at Site SU81-18 are lower than at present by a few units in response to freshwater discharge from the surrounding Fennoscandian and Laurentide ice sheets. Also from 50 to 25 ka, SSS$_{MAT}$ were lower than at present (Site MD95-2042, Penaud et al., 2011a). Furthermore, SSS$_{MAT}$ from Site MD95-2042 are consistent with the results from Site U1385 in terms of absolute SSS$_{MAT}$ values, resemblance of SSS$_{MAT}$ to SST$_{MAT}$ and distinct low salinity events during HEs (Penaud et al., 2011a). It should be noted that many dinocyst species that show a preference for warmer/colder SSTs simultaneously are indicative of higher/lower SSS (Section 3.4, Zonneveld et al., 2013), hence the observed close resemblance of SSS$_{MAT}$ and SST$_{MAT}$ is expected (Appendix C1). The correlation of salinity and temperature is a characteristic of the open ocean, but not necessarily of estuarine and epicontinental environments, where stratification and low thermal inertia result in high seasonal thermal contrasts and a wide range of salinity versus temperature relationships (cf. de Vernal et al., 2006).

The drop in SST$_{MAT}$ and SSS$_{MAT}$ at HS1 and the YD is likely related to the presence of low-salinity (sub)polar water and the melt of icebergs. Arctic and subarctic waters reached the WIM during HSs and the YD due to southward displacement of the Polar Front (e.g. Cayre et al., 1999; Bard et al., 2000; Eynaud et al., 2009). Previous studies have identified IMS-2.1a as coincident with HS1 at Sites MD95-2039/41/42 and SU81-18 along the WIM (Fig. 1), based on increased abundances of Ice Rafted Debris (IRD), peaks in magnetic susceptibility and an increase in abundances of the polar foraminiferal species *Neogloboquadrina pachyderma* (s.) (e.g. Cayre et al., 1999; Thouveny et al., 2000; Turon et al., 2003; Eynaud et al., 2009). Our SSS results corroborate

this, as the drop in SST_{MAT} corresponds to increased *N. pachyderma* abundances at Site MD95-2042 (Fig. 7G). SST_{MAT} decreases slightly less in the YD than in HS1, but this drop also corresponds to a small increase in *N. pachyderma* abundances. Hence, the protrusion of northern waters to the WIM was probably limited to subarctic waters in the YD (Eynaud et al., 2009).

5.5. Sea surface production

Accumulation rates of dinocysts sensitive to oxidation (heterotrophs) and relative abundances of *Brigantedinium* spp. were higher during the glacial stage than during the Holocene (Figs. 4 and 5H), as previously observed at sites along the WIM (Zippi, 1992; Boessenkool et al., 2001; Penaud et al., 2011b; Eynaud et al., 2016). The low abundances of S-cysts (heterotrophs) in the Holocene may be partially related to increased oxygen-mediated degradation, as indicated by relatively high kt values from ~8 ka (Fig. 4), related to lower sedimentation rates (Fig. 4 and Appendix B: Fig. B2). However, before ~8 ka kt values are low and do not vary much, while the accumulation rates of S- and R-cysts both decrease after the glacial stage (Figs. 4 and 5H), indicating that there is no large preservation bias of heterotrophic cysts. Hence, the high glacial accumulation rates of R-cysts (autotrophs), but probably also S-cysts (heterotrophs), result from increased production of the cysts, which reflects increased availability of nutrients and prey, but does not necessarily imply an increase in local upwelling (Eynaud et al., 2000).

Dinocyst MAT-based mean annual primary production (SSP_{MAT}) and planktonic foraminiferal summer exported production (P_{exp_su}, Penaud et al., 2011b; Salgueiro et al., 2010, 2014) also show generally high production in the glacial stage compared to the Holocene (Fig. 7J). Previous studies suggested that changes in productivity could be related to changes in local upwelling dynamics (e.g. Pailler and Bard, 2002; Voelker et al., 2009; Salgueiro et al., 2014) that is influenced by the intensity, persistence, spatial extent and/or nutrient availability of the upwelling filaments along the WIM (Salgueiro et al., 2010). The lower glacial sea level could have led to a westward displacement of coastal upwelling filaments (Salgueiro et al., 2010, 2014), but we consider this a minor factor because the coastline was only ~3 km closer to Site U1385 (Section 2.2). In addition, an increase in the intensity and steadiness of the northerly winds during the glacial could have led to enhanced upwelling and, consequently, productivity along the WIM (Pailler and Bard, 2002; Voelker et al., 2008; Salgueiro et al., 2010, 2014). Increased productivity could also be related to nutrient input from winds or rivers, not necessarily implying enhanced vertical mixing in the water column.

Stadial-interstadial variability is less consistent between the dinocyst- and foraminiferal SSP tracers (Figs. 5F–G and 7J). Dinocyst SSP_{MAT} indicates high SSP in HS1 and the YD, while the accumulation rate of R-cysts and foraminiferal P_{exp_su} indicate decreased SSP in HS1 and decreasing SSP in the YD. All three production tracers show low SSP at the start of the B-A. SSP_{MAT} possibly reconstructs higher SSP due to the relatively large abundance of heterotrophic cysts in HS1 and the YD. In addition to differences in the dinocyst and foraminiferal MAT-based approaches, dinocysts reflect mean annual primary production, while foraminifera reflect summer-exported production, hence differences in production signals are expected. Lower summer P_{exp} in HS1 is in agreement with southward penetration of cold iceberg-derived meltwater (Salgueiro et al., 2014). Differences and shifts in seasonality of dinoflagellates and foraminifera could explain the lower summer foraminiferal P_{exp} and relatively high mean annual dinocyst primary production.

6. Conclusions

We generated reconstructions of sea-surface parameters (SST, SSS, SSP) from IODP Site U1385 covering the last 22 kyr based on a suite of qualitative and quantitative approaches applied to dinocyst assemblages. We compared them to other reconstructions based on different approaches and/or different indicators (foraminifera, stable oxygen isotopes, alkenones) from nearby sites. Our work leads to several conclusions:

(1) Calculation of our dinocyst indicator taxa index (SST_{dino}) on assemblages of the surface sediment dataset of de Vernal et al. (2013a) and regression versus present-day SST, SSS and SSP of the same samples indicates that our qualitative dinocyst SST index mainly reconstructs SST, with only a small SSS component. The qualitative SST_{dino} and quantitative MAT reconstructions generally resemble each other as well as SST from many records based on dinocysts, alkenones and foraminifers from sites along the WIM. This implies that the ecological constraints used to develop the SST index are correct and can be applied back in time. Moreover, the MAT-based temperature reconstructions actually reflect temperature-induced changes in dinocyst ecology.

(2) The quantitative tracers based on dinocysts, alkenones and foraminifera agree on a relatively warm glacial summer, only a few degrees colder than in the Holocene. However, reconstructions for glacial winter SSTs diverge more between tracers, hence seasonality reflected in the tracers may differ between sites and over time. Increased seasonal temperature differences during the glacial from the MAT approach originate from strong winter cooling.

(3) In previous studies $U_{37}^{k'}$ temperatures are interpreted as reflecting annual mean SST or SST skewed towards the summer. $U_{37}^{k'}$ from a nearby site corresponds to annual SST based on our quantified dinocyst index, but is within error of summer SST based on MAT. With the present data it is difficult to draw a conclusion about the accuracy and seasonality of both dinocyst methods.

(4) Our new dinocyst MAT-based SSS record shows glacial-interglacial and stadial-interstadial changes in SSS concomitant with changes in SST at Site U1385 over the last 22 kyr. This is not surprising, since SSS and SST are typically related in open marine settings. SSS_{MAT} shows a clear drop during the YD and HS1 corresponding to increased *N. pachyderma* abundances at nearby Site MD95-2042.

(5) Accumulation rates of cysts resistant to oxidative degradation and MAT-based dinocyst mean annual primary production (SSP_{MAT}) show generally high production in the glacial stage compared to the Holocene, in line with previous work.

(6) The qualitative dinocyst-based SST reconstructions show larger shifts and higher variability in the Holocene than other SST tracers (dinocyst and foraminifer based MAT, $\delta^{18}O$, $U_{37}^{k'}$). The limited number of modern analogues from warm ocean regions in the reference dataset might mask variability in warm periods in our dinocyst SST_{MAT}. Alternatively, relatively small sample size for the qualitative SST_{dino} index and the possible effect of SSS might amplify noise. Also for the MAT a parameter other than SST might play a role, since the MAT reconstructs SST based on similarity of complete assemblages and not warm/cold taxa only. In addition, changes in blooming season of phytoplankton or depth habitat of foraminifera though time could have contributed to the differences between dinoflagellate-, alkenone- and foraminifer-based approaches.

(7) In any case, the advantage of the qualitative SST_{dino} approach is the possibility to make qualitative estimates even in non-analogue situations. Because the index is based on indicator taxa that are relatively warm/cold relative to local SST at Site U1385, the quantified index can only reconstruct a limited range of SSTs, especially towards lower SSTs, and with a relatively large uncertainty. However, an advantage of the quantified index is that it can reconstruct $SST_{(su)}$ beyond the upper limit of the MAT. The MAT reconstructs more reliable SSTs, with a much smaller error of prediction than the quantified index, but with the available test database only up to present-day WIM values. A limit of the MAT is

that sites closest to the site that is being investigated often have the most similar assemblages, even though the sea surface parameters of downcore assemblages are possibly more similar to sites from different regions in the reference dataset. The MAT is based on the assumption that past assemblages have modern counterparts that correspond to similar sea-surface conditions, which is not always valid. The advantages of the MAT approach include its quantitative nature and insights into seasonality. The various methods are therefore strongly complementary: at Site U1385 MAT can be used for reconstructions in the colder periods (YD, HS1 and glacial stage), with a small error of prediction and the quantified index can be used to estimate SST beyond the limit of the MAT (Holocene and B-A).

(8) Our high-resolution palynological tracer records for Site U1385 are an addition to the robust multi-proxy marine reference site for Pleistocene climate variability. Moreover, trends and events recorded in SST_{dino} and SST_{MAT} at Site U1385 over the last 22 kyr match those recognized in the oxygen isotopic composition of Greenland ice. Hence, the results support the hypothesis of teleconnection in the millennial-scale climate variability at the scale of the North Atlantic region.

Supplementary data to this article can be found online at http://dx.doi.org/10.1016/j.marmicro.2017.08.003.

Acknowledgements

References

Álvarez, M., Pérez, F.F., Bryden, H., Ríos, A.F., 2004. Physical and biogeochemical transports structure in the North Atlantic subpolar gyre. J. Geophys. Res. 109 (C03027), 1–21. http://dx.doi.org/10.1029/2003JC002015.

Arístegui, J., Álvarez-Salgado, X.A., Barton, E.D., Figueiras, F.G., Hernández-León, S., Roy, C., Santos, A.M.P., 2005. Oceanography and fisheries of the Canary Current/Iberian region of the eastern North Atlantic (18a, E). In: Robinson, Allan R., Brink, Kenneth H. (Eds.), The Sea. vol. 14.

Arístegui, J., Barton, E.D., Álvarez-Salgado, X.A., Santos, A.M.P., Figueiras, F.G., Kifani, S., Hernández-León, S., Mason, E., Machú, E., Demarcq, H., 2009. Sub-regional ecosystem variability in the Canary Current upwelling. Prog. Oceanogr. 83, 33–48. http://dx.doi.org/10.1016/j.pocean.2009.07.031.

Bard, E., Rostek, F., Turon, J.-L., Gendreau, S., 2000. Hydrological impact of Heinrich events in the subtropical Northeast Atlantic. Science 289, 1321–1324. http://dx.doi.org/10.1126/science.289.5483.1321.

Bard, E., 2001. Comparison of alkenone estimates with other paleotemperature proxies. Geochem. Geophys. Geosyst. 2 (1). http://dx.doi.org/10.1029/2000GC000050.

Barker, S., Knorr, G., Edwards, R.L., Parrenin, F., Putnam, A.E., Skinner, L.C., Wolff, E., Ziegler, M., 2011. 800,000 years of abrupt climate variability. Science 334, 347–351. http://dx.doi.org/10.1126/science.1203580.

Beug, H.-J., 2004. Leitfaden der Pollenbestimmung für Mitteleuropa und angrenzende Gebiete. Publisher Verlag Friedrich Pfeil, Munich (542 pp.).

Bischof, B., Mariano, A.J., Ryan, E.H., 2003. The Portugal current system. Ocean surface currents. http://oceancurrents.rsmas.miami.edu/atlantic/portugal.html.

Boessenkool, K.P., Brinkhuis, H., Schönfeld, J., Targarona, J., 2001. North Atlantic sea-surface temperature changes and the climate of western Iberia during the last deglaciation; a marine palynological approach. Glob. Planet. Chang. 30, 33–39. http://dx.doi.org/10.1016/S0921-8181(01)00075-3.

Bogus, K., Harding, I.C., King, A., Charles, A.J., Zonneveld, K.A.F., Versteegh, G.J.M., 2012. The composition and diversity of dinosporin in species of the *Apectodinium*

complex (Dinoflagellata). Rev. Palaeobot. Palynol. 183, 21–31. http://dx.doi.org/10.1016/j.revpalbo.2012.07.001.

Bond, G., Showers, W., Cheseby, M., Lotti, R., Almasi, P., deMenocal, P., Priore, P., Cullen, H., Hajdas, I., Bonani, G., 1997. A pervasive millennial-scale cycle in North Atlantic Holocene and glacial climates. Science 278, 1257–1266. http://dx.doi.org/10.1126/science.278.5341.1257.

Bond, G., Showers, W., Elliot, M., Evans, M., Lotti, R., Hajdas, I., Bonani, G., Johnsen, S., 1999. The North Atlantic's 1–2 kyr climate rhythm: relation to Heinrich events, Dansgaard/Oeschger cycles and the little ice age. In: AGU Geophysical Monograph. 112. pp. 35–58. http://dx.doi.org/10.1029/GM112p0035.

Boyer, T.P., Antonov, J.I., Baranova, O.K., Coleman, C., Garcia, H.E., Grodsky, A., Johnson, D.R., Locarnini, R.A., Mishonov, A.V., O'Brien, T.D., Paver, C.R., Reagan, J.R., Seidov, D., Smolyar, I.V., Zweng, M.M., 2013. In: Levitus, S. (Ed.), World Ocean Database 2013, NOAA Atlas NESDIS 72, (A. Mishonov, Technical Ed.; Silver Spring, MD, 209 pp.). http://dx.doi.org/10.7289/V5NZ85MT. http://odv.awi.de/en/data/ocean/world_ocean_atlas_2013/.

Cayre, O., Lancelot, Y., Vincent, E., 1999. Paleoceanographic reconstructions from planktonic foraminifera off the Iberian Margin: temperature, salinity, and Heinrich events. Paleoceanography 14, 384–396. http://dx.doi.org/10.1029/1998PA900027.

Cheng, H., Edwards, R.L., Broecker, W.S., Denton, G.H., Kong, X., Wang, Y., Zhang, R., Wang, X., 2009. Ice age terminations. Science 326, 248–252. http://dx.doi.org/10.1126/science.1177840.

Conte, M.H., Sicre, M., Ruhlemann, C., Weber, J., Schulte, S., Schulz-Bull, D., Blanz, T., 2006. Global temperature calibration of the alkenone unsaturation index ($U_{37}^{k\prime}$) in surface waters and comparison with surface sediments. Geochem. Geophys. Geosyst. 7. http://dx.doi.org/10.1029/2005GC001054.

Darfeuil, S., Ménot, G., Giraud, X., Rostek, F., Tachikawa, K., Garcia, M., Bard, E., 2016. Sea surface temperature reconstructions over the last 70 ky off Portugal: biomarker data and regional modeling. Paleoceanography 31, 40–65. http://dx.doi.org/10.1002/2015PA002831.(Data at: http://onlinelibrary.wiley.com/doi/10.1002/2015PA002831/abstract).

de Vernal, A., Hillaire-Marcel, C., Turon, J.-L., Matthiessen, J., 2000. Reconstruction of sea-surface temperature, salinity, and sea-ice cover in the northern North Atlantic during the last glacial maximum based on dinocyst assemblages. Can. J. Earth Sci. 37, 725–750. http://dx.doi.org/10.1139/e99-091.

de Vernal, A., Henry, M., Matthiessen, J., Mudie, P.J., Rochon, A., Boessenkool, K.P., Eynaud, F., Grøsfjeld, K., Guiot, J., Hamel, D., Harland, R., Head, M.J., Kunz-Pirrung, M., Levac, E., Loucheur, V., Peyron, O., Pospelova, V., Radi, T., Turon, J.-L., Voronina, E., 2001. Dinoflagellate cyst assemblages as tracers of sea-surface conditions in the northern North Atlantic, Arctic and sub-Arctic seas: the new 'n = 677' data base and its application for quantitative palaeoceanographic reconstruction. J. Quat. Sci. 16, 681–698. http://dx.doi.org/10.1002/jqs.659.

de Vernal, A., Eynaud, F., Henry, M., Hillaire-Marcel, C., Londeix, L., Mangin, S., Matthiessen, J., Marret, F., Radi, T., Rochon, A., Solignac, S., Turon, J.-L., 2005. Reconstruction of sea-surface conditions at middle to high latitudes of the Northern Hemisphere during the Last Glacial Maximum (LGM) based on dinoflagellate cyst assemblages. Quat. Sci. Rev. 24, 897–924. http://dx.doi.org/10.1016/j.quascirev.2004.06.014.

de Vernal, A., Rosell-Melé, A., Kucera, M., Hillaire-Marcel, C., Eynaud, F., Weinelt, M., Dokken, T., Kageyama, M., 2006. Comparing proxies for the reconstruction of LGM sea-surface conditions in the northern North Atlantic. Quat. Sci. Rev. 25, 2820–2834. http://dx.doi.org/10.1016/j.quascirev.2006.06.006.

de Vernal, A., Hillaire-Marcel, C., Rochon, A., Fréchette, B., Henry, M., Solignac, S., Bonnet, 2013a. Dinocyst-based reconstructions of sea ice cover concentration during the Holocene in the Arctic Ocean, the northern North Atlantic Ocean and its adjacent seas. Quat. Sci. Rev. 79, 111–121. http://dx.doi.org/10.1016/j.quascirev.2013.07.006.

de Vernal, A., Rochon, A., Fréchette, B., Henry, M., Radi, T., Solignac, S., 2013b. Reconstructing past sea ice cover of the Northern Hemisphere from dinocyst assemblages: status of the approach. Quat. Sci. Rev. 79, 122–134. http://dx.doi.org/10.1016/j.quascirev.2013.06.022.(http://www.geotop.ca/en/bases-de-donnees/dinokystes.html).

European Marine Observation and Data Network Portal for bathymetry. http://www.emodnet-bathymetry.eu.

Expedition 339 Scientists: Site U1385, 2013. In: Stow, D.A.V., Hernández-Molina, F.J., Alvarez Zarikian, C.A., Expedition 339 Scientists (Eds.), Proc. IODP, 339: Tokyo (Integrated Ocean Drilling Program Management International, Inc.), http://dx.doi.org/10.2204/iodp.proc.339.103.2013.

Eynaud, F., 1999. Kystes de Dinoflagellés et Evolution paléoclimatique et paléohydrologique de l'Atlantique Nord au cours du Dernier Cycle Climatique du Quaternaire (Thèse de 3e cycle). Université de Bordeaux I.

Eynaud, F., Turon, J.-L., Sanchez Goñi, M.F., Gendreau, S., 2000. Dinoflagellate cyst evidence of "Heinrich-like events" off Portugal during the marine isotopic stage 5. Mar. Micropaleontol. 40, 9–21. http://dx.doi.org/10.1016/S0377-8398(99)00045-6.

Eynaud, F., de Abreu, L., Voelker, A., Schönfeld, J., Salgueiro, E., Turon, J.-L., Penaud, A., Toucanne, S., Naughton, F., Sanchez Goñi, M.F., Malaizé, B., Cacho, I., 2009. Position of the Polar Front along the western Iberian margin during key cold episodes of the last 45 ka. Geochem. Geophys. Geosyst. 10 (7). http://dx.doi.org/10.1029/2009GC002398.

Eynaud, F., Londeix, L., Penaud, A., Sanchez-Goni, M.F., Oliveira, D., Desprat, S., Turon, J.-L., 2016. Dinoflagellate cyst population evolution throughout past interglacials: Key features along the Iberian margin and insights from the new IODP Site U1385 (Exp 339). Glob. Planet. Chang. 136, 52–64. http://dx.doi.org/10.1016/j.gloplacha.2015.12.004.(Data at: http://www.sciencedirect.com/science/article/pii/S0921818115301466?via%3Dihub#ec0005).

Govin, A., Chiessi, C.M., Zabel, M., Sawakuchi, A.O., Heslop, D., Hörner, T., Zhang, Y.,

Mulitza, S., 2014. Terrigenous input off northern South America driven by changes in Amazonian climate and the North Brazil Current retroflection during the last 250 ka. Clim. Past 10, 843–862. http://dx.doi.org/10.5194/cp-10-843-2014.

Guiot, J., de Vernal, A., de Vernal, 2007. Transfer functions: methods for quantitative paleoceanography based on microfossils. In: Hillaire-Marcel (Ed.), Proxies in Late Cenozoic Paleoceanography. Developments in Marine Geology 1. Elsevier, pp. 523–563. http://dx.doi.org/10.1016/S1572-5480(07)01018-4.

Hodell, D.A., Crowhurst, S., Skinner, L., Tzedakis, P.C., Margari, V., Channell, J.E.T., Kamenov, G., Maclachlan, S., Rothwell, G., 2013a. Response of Iberian Margin sediments to orbital and suborbital forcing over the past 420 ka. Paleoceanography 28, 185–199. http://dx.doi.org/10.1002/palo.20017.(Data at: https://www.ncdc.noaa.gov/paleo/study/15776).

Hodell, D.A., Lourens, L., Stow, D.A.V., Hernández-Molina, J., Alvarez Zarikian, C.A., Shackleton Site Project Members, 2013b. The "Shackleton Site" (IODP Site U1385) on the Iberian Margin. Sci. Drill. 16, 13–19. http://dx.doi.org/10.5194/sd-16-13-2013.

Hodell, D.A., Lourens, L., Crowhurst, S., Konijnendijk, T., Tjallingii, R., Jiménez-Espejo, F., Skinner, L., Tzedakis, P.C., Shackleton Site Project Members, 2015. A reference time scale for Site U1385 (Shackleton Site) on the SW Iberian Margin. Glob. Planet. Chang. 133, 49–64. http://dx.doi.org/10.1016/j.gloplacha.2015.07.002.(Data at: https://www.ncdc.noaa.gov/paleo/study/19782).

Hopkins, J., Henson, S.A., Painter, S.C., Tyrrell, T., Poulton, A.J., 2015. Phenological characteristics of global coccolithophore blooms. Glob. Biogeochem. Cycles 29 (2), 239–253. http://dx.doi.org/10.1002/2014GB004919.

Kucera, M., Weinelt, M., Kiefer, T., Pflaumann, U., Hayes, A., Weinelt, M., Chen, M.-T., Mix, A.C., Barrows, T.T., Cortijo, E., Duprat, J., Juggins, S., Waelbroeck, C., 2005. Reconstruction of sea-surface temperatures from assemblages of planktonic foraminifera: multi-technique approach based on geographically constrained calibration data sets and its application to glacial Atlantic and Pacific Oceans. Quat. Sci. Rev. 24, 951–998. http://dx.doi.org/10.1016/j.quascirev.2004.07.014.

Leorri, E., Fatela, F., Drago, T., Bradley, S.L., Moreno, J., Cearreta, A., 2013. Late glacial and Holocene coastal evolution in the Minho estuary (N Portugal): Implications for understanding sea-level changes in Atlantic Iberia. The Holocene 23, 353–363. http://dx.doi.org/10.1177/0959683612460786.

Lignum, J., Jarvis, I., Pearce, M.A., 2008. A critical assessment of standard processing methods for the preparation of palynological samples. Rev. Palaeobot. Palynol. 149, 133–149. http://dx.doi.org/10.1016/j.revpalbo.2007.11.004.

Martrat, B., Grimalt, J.O., Shackleton, N.J., de Abreu, L., Hutterli, M.A., Stocker, T.F., 2007. Four climate cycles of recurring deep and surface water destabilizations on the Iberian Margin. Science 317, 502–507. http://dx.doi.org/10.1126/science.1139994.

Mayewski, P.A., Rohling, E.E., Stager, J.C., Karlén, W., Maasch, K.A., Meeker, L.D., Meyerson, E.A., Gasse, F., van Kreveld, S., Holmgren, K., Lee-Thorp, J., Rosqvist, G., Rack, F., Staubwasser, M., Schneider, R.R., Steig, E.J., 2004. Holocene climate variability. Quat. Res. 62, 243–255. http://dx.doi.org/10.1016/j.yqres.2004.07.001.

Müller, P.J., Kirst, G., Ruhland, G., von Storch, I., Rosell-Melé, A., 1998. Calibration of the alkenone paleotemperature index $U^{k'}_{37}$ based on core-tops from the eastern South Atlantic and the global ocean (60°N-60°S). Geochim. Cosmochim. Acta 62, 1757–1772. http://dx.doi.org/10.1016/S0016-7037(98)00097-0.

Naughton, F., Sanchez Goñi, M.F., Desprat, S., Turon, J.-L., Duprat, J., Malaizé, B., Joli, C., Cortijo, E., Drago, T., Freitas, M.C., 2007. Present-day and past (last 25,000 years) marine pollen signal off western Iberia. Mar. Micropaleontol. 62, 91–114. http://dx.doi.org/10.1016/j.marmicro.2006.07.006.

Pailler, D., Bard, E., 2002. High frequency palaeoceanographic changes during the past 140,000 yr recorded by the organic matter in sediments of the Iberian Margin. Palaeogeogr. Palaeoclimatol. Palaeoecol. 181, 431–452. http://dx.doi.org/10.1016/S0031-0182(01)00444-8.

Peliz, Á., Dubert, J., Santos, A.M.P., Oliveira, P.B., Le Cann, B., 2005. Winter upper ocean circulation in the Western Iberian Basin—Fronts, Eddies and Poleward Flows: an overview. Deep-Sea Res. I Oceanogr. Res. Pap. 52, 621–646. http://dx.doi.org/10.1016/j.dsr.2004.11.005.

Penaud, A., Eynaud, F., Turon, J.L., Blamart, D., Rossignol, L., Marret, F., Lopez-Martinez, C., Grimalt, J.O., Malaizé, B., Charlier, K., 2010. Contrasting paleoceanographic conditions off Morocco during Heinrich events (1 and 2) and the Last Glacial Maximum. Quat. Sci. Rev. 29, 1923–1939. http://dx.doi.org/10.1016/j.quascirev.2010.04.011.

Penaud, A., Eynaud, F., Sanchez Goñi, M.F., Malaizé, B., Turon, J.L., Rossignol, L., 2011a. Contrasting sea-surface responses between the western Mediterranean Sea and eastern subtropical latitudes of the North Atlantic during abrupt climatic events of MIS 3. Mar. Micropaleontol. 80, 1–17. http://dx.doi.org/10.1016/j.marmicro.2011.03.002.

Penaud, A., Eynaud, F., Voelker, A., Kageyama, M., Marret, F., Turon, J.L., Blamart, D., Mulder, T., Rossignol, L., 2011b. Assessment of sea surface temperature changes in the Gulf of Cadiz during the last 30 ka: implications for glacial changes in the regional hydrography. Biogeosciences 8, 2295–2316. http://dx.doi.org/10.5194/bg-8-2295-2011.

R Core Team, 2015. R: A Language and Environment for Statistical Computing. R Foundation for Statistical Computing, Vienna, Austria. http://www.R-project.org/.

Radi, T., de Vernal, A., 2008. Dinocysts as proxy of primary productivity in mid–high latitudes of the Northern Hemisphere. Mar. Micropaleontol. 68, 84–114. http://dx.doi.org/10.1016/j.marmicro.2008.01.012.

Radi, T., Bonnet, S., Cormier, M.-A., de Vernal, A., Durantou, L., Faubert, É., Head, M.J., Henry, M., Pospelova, V., Rochon, A., van Nieuwenhove, N., 2013. Operational taxonomy and (paleo-)autecology of round, brown, spiny dinoflagellate cysts from the Quaternary of high latitudes. Mar. Micropaleontol. 98, 41–57. http://dx.doi.org/10.1016/j.marmicro.2012.11.001.

Rasmussen, S.O., Bigler, M., Blockley, S.P., Blunier, T., Buchard, S.L., Clausen, H.B., Cvijanovic, I., Dahl-Jensen, D., Johnsen, S.J., Fischer, H., Gkinis, V., Guillevic, M.,

Hoek, W.Z., Lowe, J.J., Pedro, J.B., Popp, T., Seierstad, I.K., Steffensen, J.P., Svensson, A.M., Vallelonga, P., Vinther, B.M., Walker, M.J.C., Wheatley, J.J., Winstrup, M., 2014. A stratigraphic framework for abrupt climatic changes during the last glacial period based on three synchronized Greenland ice-core records: refining and extending the INTIMATE event stratigraphy. Quat. Sci. Rev. 106, 14–28. http://dx.doi.org/10.1016/j.quascirev.2014.09.007.

Relvas, P., Barton, E.D., Dubert, J., Oliveira, P.B., Peliz, Á., da Silva, J.C.B., Santos, A.M.P., 2007. Physical oceanography of the western Iberia ecosystem: latest views and challenges. Prog. Oceanogr. 74, 149–173. http://dx.doi.org/10.1016/j.pocean.2007.04.021.

Ribeiro, S., Amorim, A., 2008. Environmental drivers of temporal succession in recent dinoflagellate cyst assemblages from a coastal site in the North-East Atlantic (Lisbon Bay, Portugal). Mar. Micropaleontol. 68, 156–178. http://dx.doi.org/10.1016/j.marmicro.2008.01.013.

Ribeiro, S., Amorim, A., Abrantes, F., Ellegaard, M., 2016. Environmental change in the Western Iberia Upwelling Ecosystem since the preindustrial period revealed by dinoflagellate cyst records. The Holocene 1–16. http://dx.doi.org/10.1177/0959683615622548.

Rochon, A., de Vernal, A., Turon, J.L., Matthiessen, J., Head, M.J., 1999. Distribution of Recent Dinoflagellate Cysts in Surface Sediments From the North Atlantic Ocean and Adjacent Seas in Relation to Sea-surface Parameters. American Association of Stratigraphic Palynologists Contributions Series 35. pp. 1–146.

Rodrigues, T., Voelker, A.H.L., Grimalt, J.O., Abrantes, F., Naughton, F., 2011. Iberian Margin sea surface temperature during MIS 15 to 9 (580–300 ka): Glacial suborbital variability versus interglacial stability. Paleoceanography 26. http://dx.doi.org/10.1029/2010PA001927.

Salgueiro, E., Voelker, A.H.L., de Abreu, L., Abrantes, F., Meggers, H., Wefer, G., 2010. Temperature and productivity changes off the western Iberian margin during the last 150 ky. Quat. Sci. Rev. 29, 680–695. http://dx.doi.org/10.1016/j.quascirev.2009.11.013.

Salgueiro, E., Naughton, F., Voelker, A.H.L., de Abreu, L., Alberto, A., Rossignol, L., Duprat, J., Magalhães, V.H., Vaqueiro, S., Turon, J.L., Abrantes, F., 2014. Past circulation along the western Iberian margin: a time slice vision from the last glacial to the Holocene. Quat. Sci. Rev. 106, 316–329. http://dx.doi.org/10.1016/j.quascirev.2014.09.001.

Sanchez Goñi, M.F., 2006. Interactions végétation-climat au cours des derniers 425.000 ans en Europe occidentale. Le message du pollen des archives marines. Quaternaire 17, 3–25.

Sanchez Goñi, M.F., Harrison, S.P., 2010. Millennial-scale climate variability and vegetation changes during the last glacial: concepts and terminology. Quat. Sci. Rev. 29, 2823–2827. http://dx.doi.org/10.1016/j.quascirev.2009.11.014.

Sanchez Goñi, M.F., Eynaud, F., Turon, J.L., Shackleton, N.J., 1999. High resolution palynological record off the Iberian margin: direct land-sea correlation for the last interglacial complex. Earth Planet. Sci. Lett. 171, 123–137. http://dx.doi.org/10.1016/S0012-821X(99)00141-7.

Sanchez Goñi, M.F., Eynaud, F., Turon, J.-L., Gendreau, S., 2000a. European climatic response to millenial-scale climatic changes in the atmosphere-ocean system during the last glacial period. Quat. Res. 54, 394–403. http://dx.doi.org/10.1006/qres.2000.2176.

Sanchez Goñi, M.F., Turon, J.L., Eynaud, F., Shackleton, N.J., Cayre, O., 2000b. Direct land/sea correlation of the Eemian, and its comparison with the Holocene: a high-resolution palynological record off the Iberian margin. Geol. Mijnb. (Netherlands Journal of Geosciences). 79 (2), 345–354. http://dx.doi.org/10.1017/S0016774600023702.

Sanchez Goñi, M.F., Cacho, I., Turon, J.-L., Guiot, J., Sierro, F.J., Peypouquet, J.-P., Grimalt, J.O., Shackleton, N.J., 2002. Synchroneity between marine and terrestrial responses to millennial scale climatic variability during the last glacial period in the Mediterranean region. Clim. Dyn. 19, 95–105. http://dx.doi.org/10.1007/s00382-001-0212-x.

Sanchez Goñi, M.F., Landais, A., Fletcher, W.J., Naughton, F., Desprat, S., Duprat, J., 2008. Contrasting impacts of Dansgaard– Oeschger events over a western European latitudinal transect modulated by orbital parameters. Quat. Sci. Rev. 27, 1136–1151. http://dx.doi.org/10.1016/j.quascirev.2008.03.003.

Sanchez Goñi, M.F., Landais, A., Cacho, I., Duprat, J., Rossignol, L., 2009. Contrasting intrainterstadial climatic evolution between high and middle North Atlantic latitudes: a close-up of Greenland Interstadials 8 and 12. Geochem. Geophys. Geosyst. 10, Q04U04. http://dx.doi.org/10.1029/2008GC002369.

Sanchez Goñi, M.F., Bard, E., Landais, A., Rossignol, L., d'Errico, F., 2013. Air–sea temperature decoupling in western Europe during the last interglacial–glacial transition. Nat. Geosci. 6, 837–841. http://dx.doi.org/10.1038/NGEO1924.

Sanchez Goñi, M.F., Llave, E., Oliveira, D., Naughton, F., Desprat, S., Ducassou, E., Hodell, D.A., Hernández-Molina, F.J., 2016. Climate changes in south western Iberia and Mediterranean Outflow variations during two contrasting cycles of the last 1 Myr: MIS 31–MIS 30 and MIS 12–MIS 11. Glob. Planet. Chang. 136, 18–29. http://dx.doi.org/10.1016/j.gloplacha.2015.11.006.

Sangiorgi, F., Capotondi, L., Nebout, N., Vigliotti, L., Brinkhuis, H., Giunta, S., Lotter, A.F., Morigi, C., Negri, A., Reichart, G.-J., 2003. Holocene seasonal sea-surface temperature variations in the southern Adriatic Sea inferred from a multiproxy approach. J. Quat. Sci. 18, 723–732. http://dx.doi.org/10.1002/jqs.782.

Shackleton, N.J., Hall, M.A., Vincent, E., 2000. Phase relationships between millennial-scale events 64,000-24,000 years ago. Paleoceanography 15, 565–569. http://dx.doi.org/10.1029/2000PA000513.

Shackleton, N.J., Fairbanks, R.G., Chiu, T.-C., Parrenin, F., 2004. Absolute calibration of the Greenland time scale: implications for Antarctic time scales and for Δ^{14}C. Quat. Sci. Rev. 23, 1513–1522. http://dx.doi.org/10.1016/j.quascirev.2004.03.006.

Skinner, L.C., Shackleton, N.J., 2004. Rapid transient changes in northeast Atlantic deep

water ventilation age across Termination I. Paleoceanography 19, 1–11. http://dx.doi.org/10.1029/2003PA000983.

Sprangers, M., Dammers, N., Brinkhuis, H., van Weering, T.C.E., Lotter, A.F., 2004. Modern organic-walled dinoflagellate cyst distribution offshore NW Iberia; tracing the upwelling system. Rev. Palaeobot. Palynol. 128, 97–106. http://dx.doi.org/10.1016/S0034-6667(03)00114-3.

Stow, D., Hernandez-Molina, F.J., Hodell, D., Alvarez Zarikian, C.A., 2011. Mediterranean outflow: environmental significance of the Mediterranean Outflow Water and its global implications. In: IODP Scientific Prospectus, pp. 339. http://dx.doi.org/10.2204/iodp.sp.339.2011.

Teles-Machado, A., Peliz, Á., McWilliams, J.C., Cardoso, R.M., Soares, P.M.M., Miranda, P.M.A., 2015a. On the year-to-year changes of the Iberian Poleward Current. J. Geophys. Res. Oceans 120, 4980–4999. http://dx.doi.org/10.1002/2015JC010758.

Teles-Machado, A., Peliz, Á., McWilliams, J.C., Couvelard, X., Ambar, I., 2015b. Circulation on the Northwestern Iberian Margin: vertical structure and seasonality of the alongshore flows. Prog. Oceanogr. 140, 134–153. http://dx.doi.org/10.1016/j.pocean.2015.05.021.

Telford, R.J., Li, C., Kucera, M., 2013. Mismatch between the depth habitat of planktonic foraminifera and the calibration depth of SST transfer functions may bias reconstructions. Clim. Past 9, 859–870.

Thouveny, N., Moreno, E., Delanghe, D., Candon, L., Lancelot, Y., Shackleton, N.J., 2000. Rock magnetic detection of distal ice-rafted debries: clue for the identification of Heinrich layers on the Portuguese margin. Earth Planet. Sci. Lett. 180, 61–75. http://dx.doi.org/10.1016/S0012-821X(00)00155-2.

Turon, J.-L., Lézine, A.-M., Denèfle, M., 2003. Land–sea correlations for the last glaciation inferred from a pollen and dinocyst record from the Portuguese margin. Quat. Res. 59, 88–96. http://dx.doi.org/10.1016/S0033-5894(02)00018-2.

Tzedakis, P.C., Pälike, H., Roucoux, K.H., de Abreu, L., 2009. Atmospheric methane, southern European vegetation and low-mid latitude links on orbital and millennial timescales. Earth Planet. Sci. Lett. 277, 307–317. http://dx.doi.org/10.1016/j.epsl.2008.10.027.

van Helmond, N.A.G.M., Hennekam, R., Donders, T.H., Bunnik, F.P.M., de Lange, G.J., Brinkhuis, H., Sangiorgi, F., 2015. Marine productivity leads organic matter preservation in sapropel S1: palynological evidence from a core east of the Nile River outflow. Quat. Sci. Rev. 108, 130–138. http://dx.doi.org/10.1016/j.quascirev.2014.11.014.

van Weering, T.C.E., de Stigter, H.C., Boer, W., de Haas, H., 2002. Recent sediment transport and accumulation on the NW Iberian margin. Prog. Oceanogr. 52, 349–371. http://dx.doi.org/10.1016/S0079-6611(02)00015-0.

Versteegh, G.J.M., Zonneveld, K.A.F., 2002. Use of selective degradation to separate preservation from productivity. Geology 30, 615–618. http://dx.doi.org/10.1130/0091-7613(2002)030<0615:UOSDTS>2.0.CO;2.

Voelker, A.H.L., de Abreu, L., 2011. In: Rashid, H., Polyak, L., Mosley-Thompson, E. (Eds.), A Review of Abrupt Climate Change Events in the Northeastern Atlantic Ocean (Iberian Margin): Latitudinal, Longitudinal, and Vertical Gradients. Abrupt Climate Change: Mechanisms, Patterns, and Impacts. American Geophysical Union, Washington, D.C.. http://dx.doi.org/10.1029/2010GM001021.

Voelker, A.H.L., Salgueiro, E., de Abreu, L., 2008. Southward shift of export productivity maxima during cold periods off the Western Iberian Margin. In: Symposium "Eastern Boundary Upwelling Ecosystems", Gran Canaria, . http://hdl.handle.net/10400.9/451.

Voelker, A.H.L., Abreu, L., Schönfeld, J., Erlenkeuser, H., Abrantes, F., 2009.

Hydrographic conditions along the western Iberian margin during marine isotope stage 2. Geochem. Geophys. Geosyst. 10, Q12U08. http://dx.doi.org/10.1029/2009GC002605.

Walker, M., Johnsen, S., Rasmussen, S.O., Popp, T., Steffensen, J.P., Gibbard, P., Hoek, W., Lowe, J., Andrews, J., Björck, S., Cwynar, L.C., Hughen, K., Kershaw, P., Kromer, B., Litt, T., Lowe, D.J., Nakagawa, T., Newnham, R., Schwander, J., 2009. Formal definition and dating of the GSSP (Global Stratotype Section and Point) for the base of the Holocene using the Greenland NGRIP ice core, and selected auxiliary records. J. Quat. Sci. 24 (1), 3–17. http://dx.doi.org/10.1002/jqs.1227.

Williams, G.L., Fensome, R.A., MacRae, R.A., 2017. The Lentin and Williams Index of Fossil Dinoflagellates, 2017 edition. American Association of Stratigraphic Palynologists Contributions Series 48. pp. 1097.

Wolff, E.W., Chappellaz, J., Blunier, T., Rasmussen, S.O., Svensson, A., 2010. Millennial-scale variability during the last glacial: the ice core record. Quat. Sci. Rev. 29, 2828–2838. http://dx.doi.org/10.1016/j.quascirev.2009.10.013.

Zippi, P.A., 1992. Dinoflagellate cyst stratigraphy and climate fluctuations in the eastern North Atlantic during the last 150,000 years. In: Head, M.J., Wrenn, J.H. (Eds.), Neogene and Quaternary Dinoflagellate Cyst of the North Atlantic Ocean and Adjacent Seas: Ecostratigraphy and Biostratigraphy, pp. 55–68.

Zonneveld, K.A.F., Brummer, G.-J.A., 2000. (Palaeo-)ecological significance, transport and preservation of organic-walled dinoflagellate cysts in the Somali Basin, NW Arabian Sea. Deep-Sea Res. II 47, 2229–2256. http://dx.doi.org/10.1016/S0967-0645(00)00023-0.

Zonneveld, K.A.F., Pospelova, V., 2015. A determination key for modern dinoflagellate cysts. Palynology 39 (3), 387–409. http://dx.doi.org/10.1080/01916122.2014.990115. https://www.marum.de/en/Modern_Dinocyst_Key.html.

Zonneveld, K.A.F., Versteegh, G.J.M., de Lange, G.J., 2001. Palaeoproductivity and post-depositional aerobic organic matter decay reflected by dinoflagellate cyst assemblages of the Eastern Mediterranean S1 sapropel. Mar. Geol. 172, 181–195. http://dx.doi.org/10.1016/S0025-3227(00)00134-1.

Zonneveld, K.A.F., Bockelmann, F., Holzwarth, U., 2007. Selective preservation of organic-walled dinoflagellate cysts as a tool to quantify past net primary production and bottom water oxygen concentrations. Mar. Geol. 237, 109–126. http://dx.doi.org/10.1016/j.margeo.2006.10.023.

Zonneveld, K.A.F., Versteegh, G.J.M., Kodrans-Nsiah, M., 2008. Preservation and organic chemistry of Late Cenozoic organic-walled dinoflagellate cysts: a review. Mar. Micropaleontol. 68, 179–197. http://dx.doi.org/10.1016/j.marmicro.2008.01.015.

Zonneveld, K.A.F., Versteegh, G.J.M., Kasten, S., Eglinton, T.I., Emeis, K.-C., Huguet, C., Koch, B.P., de Lange, G.J., de Leeuw, J.W., Middelburg, J.J., Mollenhauer, G., Prahl, F.G., Rethemeyer, J., Wakeham, S.G., 2010. Selective preservation of organic matter in marine environments; processes and impact on the sedimentary record. Biogeosciences 7, 483–511. http://dx.doi.org/10.5194/bg-7-483-2010.

Zonneveld, K.A.F., Marret, F., Versteegh, G.J.M., Bogus, K., Bonnet, S., Bouimetarhan, I., Crouch, E., de Vernal, A., Elshanawany, R., Edwards, L., Esper, O., Forke, S., Grøsfjeld, K., Henry, M., Holzwarth, U., Kielt, J.F., Kim, S.Y., Ladouceur, S., Ledu, D., Chen, L., Limoges, A., Londeix, L., Lu, S.H., Mahmoud, M.S., Marino, G., Matsouka, K., Matthiessen, J., Mildenhal, D.C., Mudie, P., Neil, H.L., Pospelova, V., Qi, Y., Radi, T., Richerol, T., Rochon, A., Sangiorgi, F., Solignac, S., Turon, J.L., Verleye, T., Wang, Y., Wang, Z., Young, M., 2013. Atlas of modern dinoflagellate cyst distribution based on 2405 data points. Rev. Palaeobot. Palynol. 191, 1–197. http://dx.doi.org/10.1594/PANGAEA.818280.